Available online at www.sciencedirect.com
SCIENCE DIRECT
Coordination Chemistry Reviews 250 (2006) 1514–1529
COORDINATION CHEMISTRY REVIEWS
www.elsevier.com/locate/ccr

Review

EPR of molecular nanomagnets

Dante Gatteschi [a,*], Anne Laure Barra [b], Andrea Caneschi [a], Andrea Cornia [c], Roberta Sessoli [a], Lorenzo Sorace [a]

[a] *INSTM & Department of Chemistry, University of Florence, Via della Lastruccia 3, 50019 Sesto Fiorentino, Italy*
[b] *Laboratoire des Champs Magnetiques Intenses-CNRS, BP166, 25 Avenue des Martyrs, 38042 Grenoble Cedex 9, France*
[c] *INSTM & Department of Chemistry, University of Modena and Reggio Emilia, via G. Campi 183, 41100 Modena, Italy*

Received 24 October 2005; accepted 8 February 2006
Available online 23 February 2006

Contents

Abstract

Electron paramagnetic resonance has played a crucial role in the determination of the properties and in explaining the origin of the peculiar behaviour of molecular nanomagnets, i.e., the slow relaxation of the magnetization at low temperature and the observation of quantum tunnelling of the magnetization. This is due to its ability to probe directly the spin levels rather than providing thermodynamic averages as in standard magnetic measurements. In particular, thanks to recent technical improvements in both reliability and sensitivity, high-field high-frequency EPR has gained widespread use for the characterization of these systems. We will briefly review here the different aspects underlying the use of this technique, highlighting some results of general interest obtained in the last decade on different class of magnetic clusters.

Keywords: Molecular nanomagnets; High frequency EPR; Magnetic properties; Magnetic anisotropy

1. Introduction

Major scientific achievements of the last few years can be labelled as the development of nanoscience and nanotechnology. The definition of the field is difficult, but a reasonable approximation can be provided by the following: research and technology development at atomic, molecular or macromolecular levels in the length scale of approximately 1–100 nm; creating and using structures, devices and systems that have novel properties and functions because of their small and/or intermediate size; ability to control and manipulate on the atomic scale [1]. The properties which are addressed are extremely different from one another, and among them magnetism certainly has an extremely important role. The interest in nanomagnetism has many different origins, ranging from novel ways of information storage to the observation of the coexistence of quantum and classical effects.

In order to investigate in depth the magnetic properties it is crucial that the magnetic particles are all identical to each other. This point becomes immediately clear if one considers the

* Corresponding author.
E-mail address: dante.gatteschi@unifi.it (D. Gatteschi).

0010-8545/$ – see front matter © 2006 Elsevier B.V. All rights reserved.
doi:10.1016/j.ccr.2006.02.006

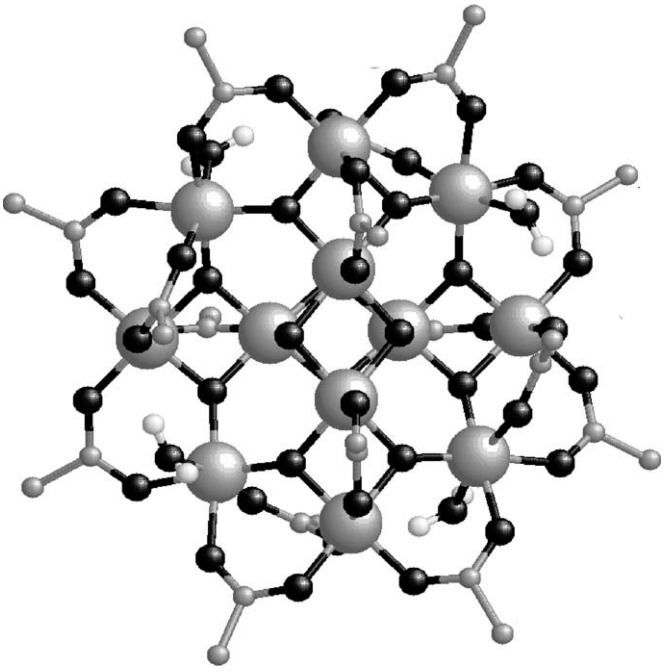

Fig. 1. Molecular structure of the archetypal single molecule magnet, Mn12Ac. Large grey spheres: Mn atoms; small grey spheres: carbon atoms; small black spheres: oxygen atoms; white spheres: hydrogen atoms. Solvent molecules and methylic hydrogen atoms are omitted for the sake of clarity.

possibility to observe quantum tunnelling of the magnetization, a typical quantum effect which can be associated with nano-size magnets. The response of the system to external stimuli scales exponentially with the size of the particles, therefore perfect monodispersity is absolutely a must if a significant measurement has to be performed [2,3]. Several different approaches have been used to prepare monodisperse magnetic particles and exciting results have been achieved, including the possibility of assembling ordered arrays of nanoparticles, the so-called nanocrystals [4–6]. In this case particles of traditional magnetic materials, like iron oxides for instance, are obtained by carefully controlling the conditions for precipitation from solution.

An alternative approach is based on coordination chemistry and consists in using large molecules, which contain a large number of interacting magnetic centres, like the dodecanuclear manganese compound depicted in Fig. 1. Its formula is $[Mn_{12}O_{12}(CH_3COO)_{16}(H_2O)_4]\cdot 4H_2O\cdot 2CH_3COOH$, Mn12Ac. The molecule was reported in 1980 and its magnetic properties studied in detail at the beginning of the 1990s [7–10]. The discovery that at low temperature the magnetization of Mn12Ac relaxes very slowly, with characteristic times which become of the order of a few months, showed that a single molecule can become a tiny magnet, and the term single molecule magnet (SMM) was suggested [11]. A whole new field of research was born, which can be called molecular nanomagnetism, consisting in the design, synthesis and investigation of the magnetic properties of large molecules [12]. The number of SMMs rapidly increased, and many different types of zero-dimensional molecular magnets are now available [13–31]. Another key development was the discovery that one-dimensional magnets may also show slow relaxation of the magnetisation at low temperature. These new systems were called single chain magnets (SCM) [32–39].

The investigation of the molecular nanomagnets requires the use of many different techniques, in order to obtain an efficient view on the nature of the ground and of the low lying spin levels [40]. Obviously the measurement of the temperature dependence of the magnetic properties, in both dc and ac modes and in varying magnetic fields is of paramount importance. A recent review is available on non-standard magnetic techniques, like microSQUID magnetometry, torque magnetometry, etc. which have gained widespread use in the last few years [41].

Not unexpectedly magnetic resonance techniques have had a key role in the interpretation of the properties of molecular nanomagnets, because they can provide a direct observation of the spin levels rather than probing thermodynamic averages, as with traditional magnetic measurements. In fact electron paramagnetic resonance (EPR) has had a tremendous impact in this field. It was only after the observation of a large negative zero field splitting in the ground $S = 10$ state that the slow relaxation of the magnetization in Mn12Ac could be clearly associated with the presence of a huge anisotropy barrier which hampers the magnetic moment reversal.

The wide use of EPR in the investigation of molecular nanomagnets has been favoured by several instrumental developments, like high frequency EPR and frequency swept magnetic resonance spectroscopy which made possible the quasi routine investigation of systems with large spins and large zero field splittings.

All the different aspects will be briefly reviewed here, not attempting to be comprehensive, because some exhaustive reviews are already available in the literature, but highlighting some important results that, in our opinion, have great pedagogical value.

2. EPR in a nutshell

Standard EPR measures the transitions between spin levels M and $M \pm 1$ of a given multiplet S split by a static magnetic induction B, induced by a quantum of radiation

$$h\nu = g\mu_B B \tag{1}$$

The quantum of radiation is in the microwave range, and for technical reasons the experiment is performed at fixed frequency by sweeping the magnetic field. The oscillating magnetic field of the radiation is usually perpendicular to the static magnetic field. Other possible geometries which give rise to different selection rules will be briefly discussed in the following. The frequency ranges (bands) are usually referred to with capital letters. The most common bands are shown in Table 1. For historical reasons, mainly bound to the ease of use of electromagnets producing few thousand Gauss and to the availability of appropriate microwave generators, X-band frequency ($\nu \sim 9$ GHz) is the most frequently used. However this frequency range has severe drawbacks when the systems investigated have $S > 1/2$. In fact in this case the S multiplet is split in zero field (zero field splitting, ZFS) by low symmetry components of the crystal field. The energies of the

Table 1
Representative EPR microwave frequencies with associated wavelengths, energies and magnetic fields for resonance at $g = 2$

ν (GHz)	λ (mm)	E (cm^{-1})	B_r ($g = 2$) (T)
9.5 (X-band)	31.5	0.317	0.34
24 (K-band)	12.5	0.8	0.86
35 (Q-band)	8.55	1.17	1.25
95 (W-band)	3.15	3.17	3.4
130 (D-band)	2.31	4.33	4.6
190	1.58	6.33	6.8
245	1.22	8.17	8.75
330	0.91	11	11.8
570	0.52	19	20.4
1000	0.3	33.3	35.7

levels can be calculated through the Hamiltonian:

$$H = \mu_B \widehat{\mathbf{S}} \cdot \mathbf{g} \cdot \widehat{\mathbf{B}} + \widehat{\mathbf{S}} \cdot \mathbf{D} \cdot \widehat{\mathbf{S}} \quad (2)$$

which can be expanded in parametric form in:

$$H = \mu_B \widehat{\mathbf{S}} \cdot \mathbf{g} \cdot \widehat{\mathbf{B}} + D\left[\widehat{S}_z^2 - \frac{S(S+1)}{3}\right] + E(\widehat{S}_x^2 - \widehat{S}_y^2) \quad (3)$$

The first term is the Zeeman term, the second and third are the crystal field (or ZFS) terms. D and E are zero for cubic symmetry, while only E is zero for axial symmetry. The sign of D reflects the type of magnetic anisotropy associated with the S multiplet. Positive D means that the $M = 0$ (for integer S) or $M = \pm 1/2$ (for half-integer S) states have the lowest energy. In these states the spin vector has the smallest component along the quantization axis (z), i.e., $\widehat{\mathbf{S}}$ lies preferentially close to the xy plane (XY-type anisotropy). On the other hand, for negative D the $M = \pm S$ states, in which $\widehat{\mathbf{S}}$ has the largest component along z, lie lowest in energy (Ising-type anisotropy).

In molecular nanomagnetism one is interested at the presence of several exchange-coupled spins. At the simplest possible level the exchange interaction can be described by a Heisenberg Hamiltonian:

$$H = \sum_{i<k} J_{ik} \widehat{\mathbf{S}}_i \cdot \widehat{\mathbf{S}}_k \quad (4)$$

The spin levels resulting from (4) are grouped into multiplets, each with a well-defined value of S, the quantum number associated with the total spin $\widehat{\mathbf{S}}$:

$$\widehat{\mathbf{S}} = \sum \widehat{\mathbf{S}}_i \quad (5)$$

In many cases (4) represents the dominant term in the spin Hamiltonian and, consequently, exchange multiplets can still be recognized in the manifold of spin levels. However, the smaller terms in the spin Hamiltonian (local anisotropies, Zeeman interactions, etc.) remove the $(2S + 1)$ degeneracy of exchange multiplets, in a way that can be very conveniently described by an effective Hamiltonian like (2) acting *within* each multiplet.

The ZFS and **g** tensors appearing in the effective Hamiltonian (2) are linearly related to the individual single-ion ZFS and **g** tensors through expressions of the type:

$$\mathbf{g}_S = \sum c_i \mathbf{g}_i \quad (6)$$

$$\mathbf{D}_S = \sum d_i \mathbf{D}_i + \sum d_{ij} \mathbf{D}_{ij} \quad (7)$$

where c_i, d_i and d_{ij} are coefficients depending on S and S_i which can be calculated through recursive relations, $\mathbf{D}_i$'s are the single ion zero field splitting tensors and $\mathbf{D}_{ij}$'s are the anisotropic spin–spin pairwise interaction tensors [42].

Within a given S multiplet several different regimes can occur depending on the relative weight of the Zeeman and ZFS terms. In the strong field limit, i.e., when the Zeeman term is much larger than the ZFS the resonant fields can be easily expressed for the case of axial symmetry. For a given field orientation $2S$ allowed transitions are observed (fine structure) and the resonant fields are given by:

$$B_r(M \rightarrow M+1) = \frac{g_e}{g}\left[B_0 - D'\frac{2M+1}{2}(3\cos^2\theta - 1)\right] \quad (8)$$

where $D' = D/(g_e \mu_B)$, and θ is the angle between the static magnetic field and the unique axis. g is Landè factor for the system under investigation while g_e is the free electron value [43].

If the strong field conditions do not apply the resonant fields cannot be analytically calculated and they must be obtained by matrix diagonalisation. Several general programs are available [44–47]. Even more important is the fact that the number of observed transitions dramatically decreases on decreasing the energy of the microwave quantum as shown in Fig. 2. The use of high frequencies is especially needed in the area of molecular nanomagnets, where large spins and large ZFS are often observed. Commercial spectrometers reach 95 GHz maximum, but experiments performed with frequencies as high as 525 GHz

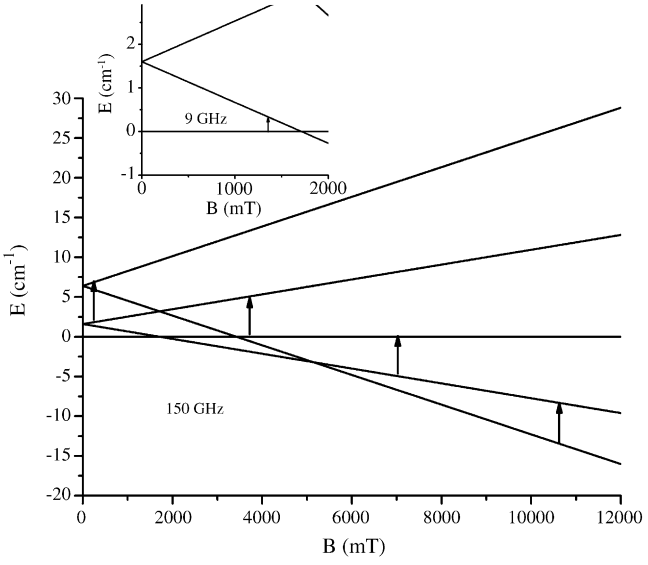

Fig. 2. Comparison of observed transitions using high-field high-frequency EPR ($B = 0$–12 T, $\nu = 150$ GHz, main graph) and conventional EPR ($B = 0$–2 T, $\nu = 9$ GHz, inset) for a system with $S = 2$ and $D = +1.6$ cm^{-1} and B/z. Only one transition is observed for the latter while all the four expected transitions can be observed by HF-EPR.

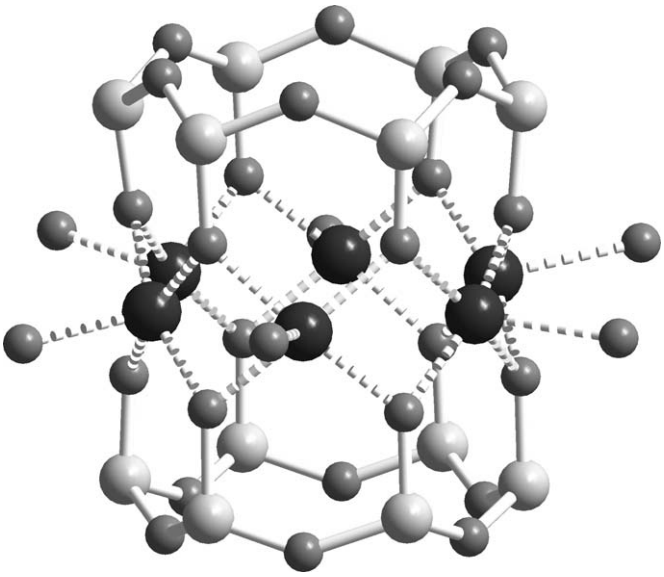

Fig. 3. Molecular structure of $[(PhSiO_2)_6Cu_6(O_2SiPh)_6]\cdot 6EtOH$, Cu6. Large black spheres: Cu atoms; large grey spheres: Si atoms; small dark grey spheres: oxygen atoms. Carbon and hydrogen atoms are omitted for the sake of clarity.

have been reported. The main advantages of working at high frequency can be summarised as follows: [48] (i) increased resolution; (ii) increased sensitivity; (iii) simplification of the spectra and of their assignment; (iv) observation of the spectra of so-called EPR silent species; (v) determination of the sign of the zero field splitting anisotropy.

Some of these points will be adequately discussed through an example. Polysiloxanolates are well known ligands able to stabilise polynuclear transition-metal ion complexes [49–52]. The structure of a hexacopper(II) derivative $[(PhSiO_2)_6Cu_6(O_2SiPh)_6]\cdot 6EtOH$, hereafter Cu6, is shown in Fig. 3 [51]. The coupling between the copper(II) metal ions, $S_i = 1/2$ is ferromagnetic so that the ground state corresponds to a configuration with all the individual spins parallel to each other. The symmetry is axial ($E = 0$) and it is possible to calculate analytically the energy levels of the $S = 3$ ground manifold by using Eq. (3). From the analysis of the spectral data it is found $g_\parallel = 2.055$; $g_\perp = 2.221$, $D/k = 0.43$ K. The polycrystalline powder spectra of Cu6 at 9 and 245 GHz are shown in Fig. 4. At 9 GHz only three partially structured transitions are observed, with a transition close to zero field, which suggests that the separation in zero field of some levels is close to the microwave quantum, namely ca. 0.3 cm^{-1}. This datum is confirmed by the high frequency spectra which show a regular fine structure, with a separation between neighbouring features of ca. 0.64 T for the parallel and ca. 0.32 T for the perpendicular features. Parallel and perpendicular refer to the unique axis.

The spectra of Fig. 4 deserve some further comment. The relative intensities of the transitions, in the hypothesis of equal population of the M levels, should follow the Fermi golden rule:

$$I(M \rightarrow M+1) \propto [(S-M)(S+M+1)] \quad (9)$$

If we look at the relative intensity of the parallel features we see that on decreasing temperature the high field transitions gain intensity. This is due to the effects of thermal depopulation of excited levels. In the EPR experiment the difference in energy between neighbouring M levels is of the order of the microwave quantum, which for the 245 GHz experiment corresponds to ca. 12 K. Therefore, when recorded at low temperature the EPR line originating from the transition $M = -S \rightarrow -S+1$ increases its intensity compared to the others. If it occurs at high field the zero field splitting is positive. The reverse situation is encountered for a negative ZFS.

Although the use of high frequency EPR spectrometers is very important it cannot be neglected that the instrumental difficulties are far from being solved. Problems are present in choosing the right source, the detection technique and the detector. After initial attempts to use far infrared lasers there is now a general trend to use solid state sources. Also, while in conventional EPR high sensitivity is achieved by using resonant cavities, this solution is difficult to implement at high frequencies due to the small size of the required cavities [53]. Quasi optical techniques have allowed important improvements [54]. Recently cavity perturbation techniques have shown that it is possible to detect the resonances even in small single crystals, without distortions [55]. In fact at the beginning people were happy even with the observation of a distorted line which allowed one to obtain a reasonable approximation of the transition fields while in the recent years high frequency EPR has rapidly become comparable to traditional experiments in terms of reliability. In this respect recent interesting developments of the technique based on magnetization measurements, either through SQUID

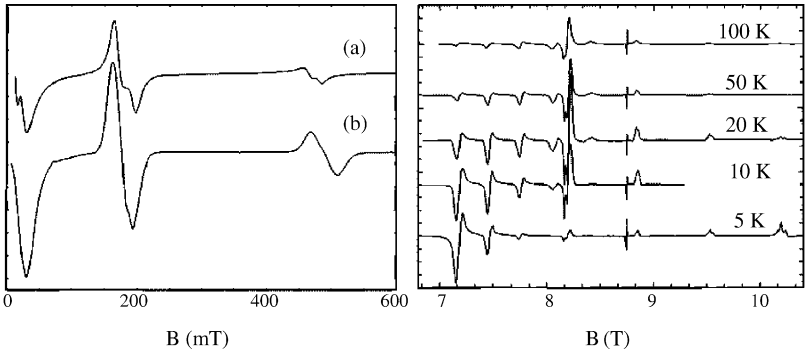

Fig. 4. (Left) Experimental (a) and simulated (b) X-Band EPR spectra of Cu6 at 4 K. (Right) Temperature evolution of the experimental HF-EPR spectra (245 GHz) of Cu6. The sharp signal at 8.8 T is DPPH signal used as reference for $g = 2.00$. Adapted from ref. [51].

or micro-Hall bar detection should be mentioned [56,57]. This approach obviates several experimental difficulties inherent to HF-EPR and exhibits an extraordinary sensitivity, being suitable for measurements of single micrometer-sized crystals.

3. EPR of Mn12Ac and related compounds

The structure of Mn12Ac was shown in Fig. 1. The crystal structure showed that the Mn12 cluster has S_4 symmetry. The eight manganese(III) ions, $S = 2$, are antiferromagnetically coupled to the four manganese(IV), $S = 3/2$, to give a ground $S = 10$ state. This is characterised by a large negative zero field splitting which leaves the $M = \pm 10$ lying lowest, determining a very large Ising-type magnetic anisotropy. In fact the EPR spectra were of capital relevance to understand the origin of the large magnetic anisotropy [8]. Polycrystalline powder spectra were measured at different frequencies, allowing to determine a zero field splitting parameter $D/k = -0.65$ K. In order to obtain reliable values of the parameters polycrystalline powder spectra were recorded at 525 GHz using a hybrid magnet (resistive plus superconducting) for the static field and a far infrared laser for the microwave frequency, Fig. 5 [58]. The central field corresponds to ca 18 T. The low field features correspond to parallel transitions, while the high field features correspond to perpendicular transitions. This is a clear evidence of a negative zero field splitting. The assignment of the low field transitions is trivial, corresponding to $M = -10 \rightarrow -9$, $-9 \rightarrow -8$, $-8 \rightarrow -7$ and $-7 \rightarrow -6$. The thermal energy corresponding to the microwave quantum is 24 K, therefore large deviations from the pattern suggested by Eq. (9) must be expected at relatively high temperature, as confirmed by the experimental data.

According to Eq. (8) the separation between neighbouring parallel lines should be $2D'$, independent of M. The experimental spectra are only in approximate agreement with this prediction. In fact additional terms must be in principle added to the Hamiltonian (2), among which presumably the most important are the fourth order terms. A convenient form for the latter in tetragonal symmetry is [59]:

$$H = B_4{}^0\widehat{\mathbf{O}}_4^0 + B_4{}^4\widehat{\mathbf{O}}_4^4 = B_4{}^0\{35\widehat{S}_z^4 - [30S(S+1) - 25]\widehat{S}_z^2 + 3S^2(S+1)^2 - 6S(S+1)\} + \frac{1}{2}B_4{}^4(\widehat{S}_+^4 + \widehat{S}_-^4) \quad (10)$$

where $\widehat{S}_+$ and $\widehat{S}_-$ are the raising and lowering operators, respectively, and $B_4{}^0$ and $B_4{}^4$ are parameters to be obtained from the analysis of experimental data. It should be noticed that introducing the term in $B_4{}^0$ adds an operator in $\widehat{S}_z^2$ which is also present in (3). Therefore, adding (10) to (3) requires a modification in the value of D. If we call D_4 the second order ZFS parameter employed when including the $\widehat{\mathbf{O}}_4^0$ term in the Spin Hamiltonian its relation with the original D is then:

$$D_4 = D + [30S(S+1) - 25]B_4{}^0 \quad (11)$$

The effect of the term in $\widehat{S}_z^4$ is that of introducing a correction to the energies of the M levels, in such a way that EPR lines arising from parallel transitions are no longer equally spaced.

An alternative to the high frequency EPR approach is that of using zero field EPR spectroscopy [60]. Indeed in the last years it has been possible to use sufficiently intense sources capable of producing microwave radiation of variable frequency. In this case it is possible to run an EPR experiment using a static field and scanning the frequency, like in an NMR experiment. Measurements performed on polycrystalline powder Mn12Ac samples clearly showed transitions which confirmed the values of the parameters obtained by EPR spectra [61]. Similar conclusions were obtained through inelastic neutron scattering, INS, experiments [62,63].

Single crystal EPR spectra were reported by Hill and coworkers, confirming the pattern of parameters associated with the crystal field effects [64,65]. These spectra further provided useful information on the role of disorder in the relaxation mechanism of the clusters.

It is perhaps useful to make a detour here to discuss some open issues on the mechanism of relaxation of the Mn12Ac clusters and then discuss the role of disorder. The anomalous slow relaxation of Mn12Ac is usually justified referring to the graph of Fig. 6. Since the magnetic behaviour of Mn12Ac is akin to that of superparamagnets [66] it is common to plot the energies of the split states of the ground $S = 10$ state in a double well, in which the energies of the negative M states are shown in the left well and those of the positive M levels are plotted in the right well. The presence of discrete levels is a clear indication of the quantum nature of the system.

At low temperature only the $M = \pm 10$ levels will be populated. If the system is prepared by saturating the magnetization, all the molecules will be in the ground $M = -10$ state. When the field is switched off thermal equilibrium will be re-established when the $M = -10$ and $+10$ states will have the same population. In order to do that it is necessary that the whole ladder of levels is climbed, with an activation energy which corresponds to the difference in energy Δ between $M = \pm 10$ and 0. An extension

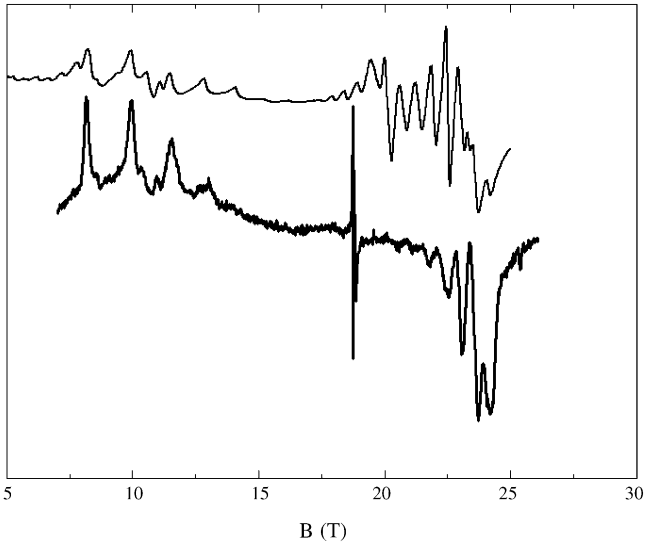

Fig. 5. Experimental (lower) and simulated (upper) 525 GHz EPR powder spectra of Mn12Ac at 30 K. Adapted from ref. [12].

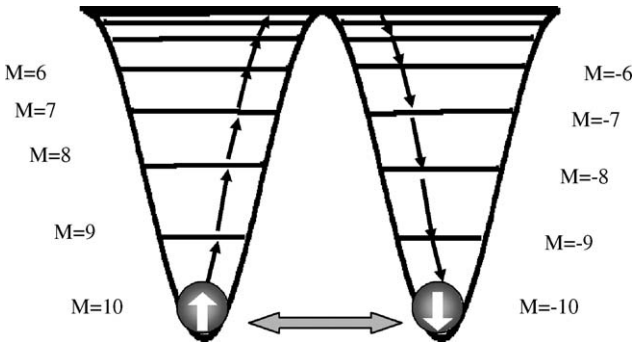

Fig. 6. Energy pattern of M sublevels for a spin state $S = 10$ and easy axis anisotropy in zero field, evidencing the two possible mechanism for magnetization reversal: through a thermally activated process (black arrows) or by quantum tunnelling (grey arrow) shortcutting the energy barrier.

of the Orbach process provides in fact the relaxation time τ indicated below:

$$\tau = \tau_0 \exp\left(\frac{\Delta}{kT}\right) \tag{12}$$

It is also possible for the spin not to climb the whole ladder but to "tunnel" through the barrier. In fact a transition from an excited $-M$ level to the corresponding $+M$ level can be promoted by transverse magnetic fields provided that $2M$ is small. This process is called thermally activated tunnelling [67,68].

A central issue is the origin of the transverse field which promotes the tunneling. In purely tetragonal symmetry, as in Mn12Ac, only the quartic term $(1/2)B_4{}^4(\widehat{S}_+^4 + \widehat{S}_-^4)$ produces a transverse field, but it admixes only states whose difference in $M \pm 4$. Therefore, the tunnel effect should be observed only for pairs of levels whose M values differ by ± 4. On the contrary the experimental results clearly indicate that relaxation through tunnelling is operative for all pairs of levels and this requires some additional transverse field to be available. One possibility was discussed by Chudnovsky and Garanin [69] who suggested that dislocations have a crucial role in the mechanism. An alternative origin was suggested by Cornia et al. [70] who re-analysed the X-ray crystal structure of Mn12Ac [71]. In fact the acetic acid molecule of solvation is disordered on a binary axis in such a way that the crystal can be described as a mixture of clusters with $n = 4$, 3, 2, 1, and 0 hydrogen-bound acetic acid molecules. Therefore, only clusters with $n = 4$ and 0 have rigorous fourfold symmetry.

The problem of the disorder has been intensively investigated by Hill et al. and del Barco et al. through single crystal EPR experiments at different frequencies [65,72–74]. In Fig. 7 is shown the variation of the linewidths and of the line splitting observed in the tetragonal plane. The splitting is attributed to the presence of distorted molecules. The fact that on the average they follow tetragonal symmetry is taken as an evidence of the presence of statistically distributed distorted molecules. Single crystal experiments have also provided some evidence for transitions originating from an excited $S = 9$ state [75,76] which was determined to lie about 40 K above the $S = 10$, $M = \pm 10$ state, a value which is in rough agreement with that determined by INS

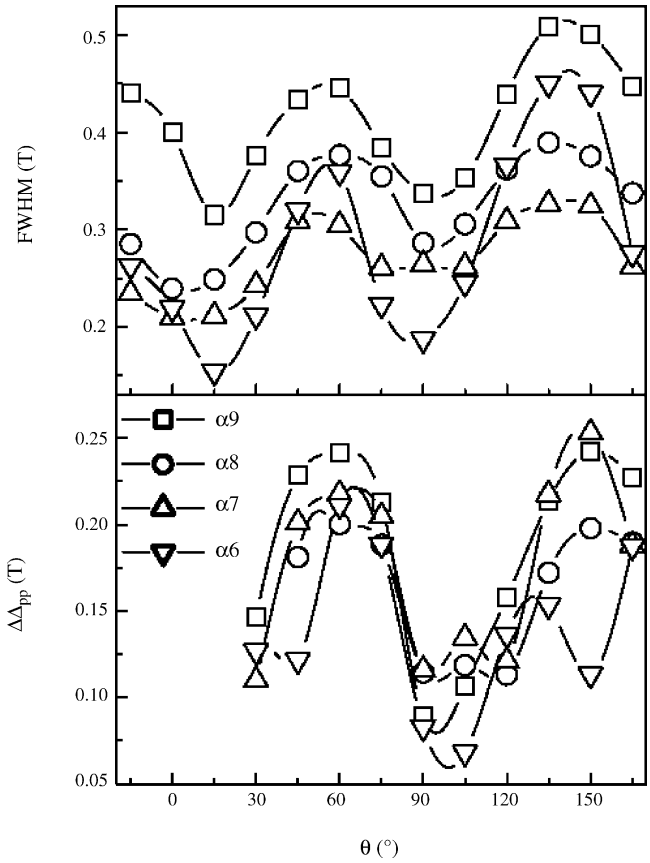

Fig. 7. Angular variation of the linewidths (upper) and of the line splitting due to the presence of different isomers (lower) observed for the four strongest EPR transitions ($\nu = 49.86$ GHz, $T = 15$ K) of Mn12Ac with static magnetic field lying in the tetragonal plane. Adapted from ref. [65].

($\Delta E \approx 60$ K) [77]. The ZFS of this state was further suggested to be very similar to that of the ground $S = 10$ state [76].

An additional problem in the interpretation of the magnetic properties of Mn12Ac is represented by the presence of a minority species, which relaxes more rapidly than the majority one. In the accepted understanding of the phenomenon this is due to the presence of largely distorted clusters. In fact the distorted molecules have a much smaller energy barrier Δ than the undistorted one. There is general agreement that the origin of the anisotropy barrier is the large Jahn–Teller distortion around the manganese(III) ions. In the majority species of Mn12Ac the local Jahn–Teller axes are essentially parallel to each other, thus maximizing the energy barrier. It is generally understood that in the minority species at least one local elongation axis has changed its orientation moving from the z-axis to the xy plane. In this way the effective barrier is reduced because it would tend to orient the spin in the plane rather than along the axis. Similar geometries have been reported for Mn12 derivatives obtained with different carboxylates. EPR information on the minority species has been reported by Takeda et al. [78].

As a very interesting feature, Mn12Ac is stable in solution and can easily be derivatized by ligand exchange [10,79–86]. It is also possible to reduce Mn12 clusters obtaining species with four manganese(IV), seven manganese(III), and one manganese(II)

ion [87]. For instance $(PPh_4)[Mn_{12}O_{12}(O_2CEt)_{16}(H_2O)_4]$, which crystallizes in the monoclinic $P2_1/c$ space group, was shown by magnetic measurements to have a ground $S = 19/2$ state [88]. The monoclinic unit cell generates some problem, because there are two magnetically inequivalent molecules. Magnetically inequivalent means that the two molecules are identical to each other (they are reported by a binary axis) but the axes of their tensors are differently oriented in the unit cell. HF EPR spectra were measured on polycrystalline powders taking advantage of the orienting effect provided by the magnetic field on such anisotropic system. It is assumed that the crystals will orient parallel to the easy axis of the crystal, which is not the easy axis of the molecule. Indeed the splitting of the fine structure components was found to correspond to an effective observed ZFS parameter D/k equal to -0.62 K. Assuming that the principal axis of the molecule makes an angle of 29° with the "monoclinic" axis, the "molecular" D value can be calculated as -0.89 K, considering that the angular dependence of the D value is of the $(3\cos^2\theta - 1)/2$ type [89].

4. Fe8

The number of SMMs has rapidly increased in the last few years, following on one hand the developments in Mn12 chemistry and on the other the discovery of completely new families of SMMs. An important achievement was the detection of SMM behavior in the so-called Fe8Br ($[Fe_8O_2(OH)_{12}(tacn)_6]Br_8\cdot 9H_2O$, where tacn = 1,4,7-triazacyclononane), a cluster completely unrelated to the Mn12 class [13,90]. Fe8Br was originally reported by Wieghardt et al., and has the structure shown in Fig. 8 [90]. The eight iron(III), $S_i = 5/2$, are antiferromagnetically coupled to give an $S = 10$ ground state, but the symmetry of the cluster is C_1 crystallising in a triclinic cell. However, the effective molecular symmetry is not far from D_2. Polycrystalline powder EPR spectra suggested $D = -0.21$ cm^{-1}, $E/D = 0.2$, where E is defined in (3). As in Mn12Ac, the negative D parameter results in an Ising-type magnetic anisotropy and, consequently, in an anisotropy barrier which slows down the relaxation of the magnetisation. At variance with Mn12Ac, the anisotropy barrier is lower and the presence of a sizeable E determines a transverse field which concurs to give a fast relaxation of the magnetization [91].

Single crystal spectra were also reported, which provided the direction of the easy axis, which as expected lies close to the perpendicular to the plane of the molecule (ca. 10° tilted with respect to this direction). The intermediate axis passes through Fe1 and Fe2, corresponding to one of the idealized C_2 axes of the cluster [92]. The directions of the anisotropy axes obtained by HF-EPR with respect to the molecular structure are reported in Fig. 8. More accurate measurements were made possible by the sensitive cavity perturbation technique, which allowed also the study of the lineshape [93]. In Fig. 9 is shown a part of the spectrum of a single crystal with the magnetic field making an angle of ca. 8° with the easy axis at a frequency of 89.035 GHz. The best fit was obtained for a Gaussian lineshape. The lines are observed to become broader with increasing $|M|$ value for the corresponding transition. In particular, the linewidth scales almost linearly with $|M|$, as expected for D-strain effects. The slight decrease of the linewidth observed on increasing frequency has been attributed to the decrease of the inter-cluster dipolar broadening. As for Mn12, some evidence for a low lying $S = 9$ multiplet ($\Delta E \cong 24$ K) with a D value comparable to that for the $S = 10$ state has been provided by these measurements [94].

Using chemical techniques it has been possible to obtain a second derivative, hereafter Fe8pcl, where about four bromide ions are substituted by perchlorate anions while essentially

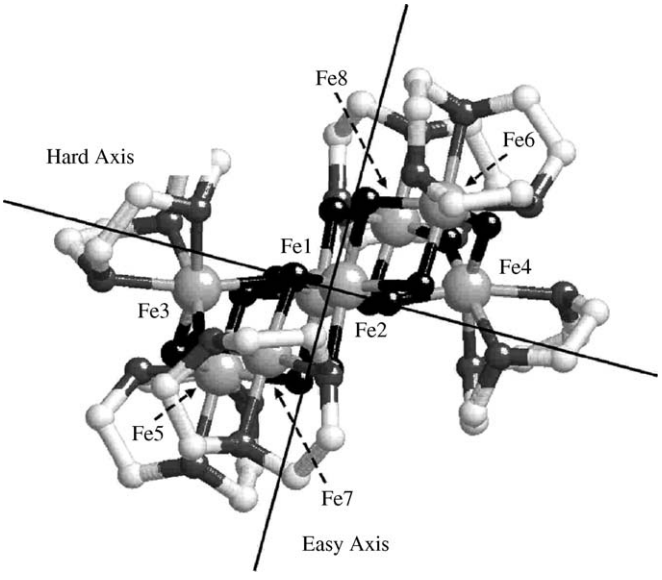

Fig. 8. Molecular structure of Fe8Br cluster showing the orientation of the hard and easy magnetic anisotropy axes as determined by single crystal HF-EPR spectra. The iron atoms are represented by large grey balls. Oxygen, carbon and nitrogen atoms are represented by small black, white and grey spheres, respectively. Adapted from ref. [92].

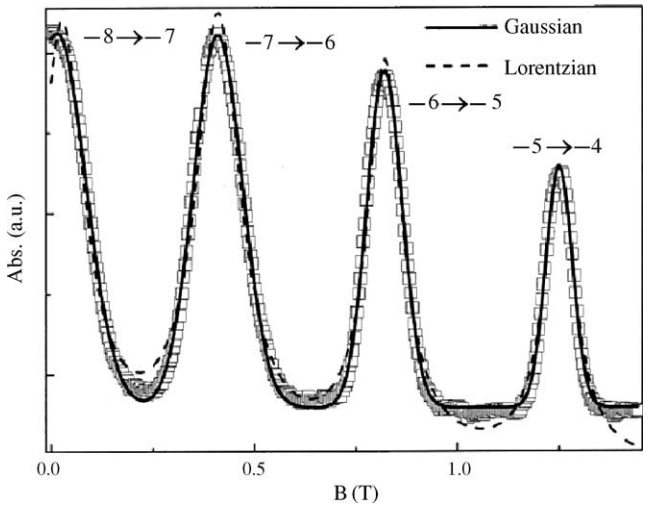

Fig. 9. Single crystal EPR spectrum ($\nu = 89.035$ GHz) of Fe8 at 10 K in absorption mode and magnetic field oriented at ca. 8° from the easy axis. Continuous and dashed lines represent the best fit obtained by using Gaussian and Lorentzian lineshape, respectively. Adapted from ref. [72].

maintaining the same core structure. Like the original derivative, Fe8pcl has been characterized by both HF-EPR and dynamic magnetic measurements [95]. The comparison of the zero-field splitting parameters determined for the two clusters by HF-EPR showed that while the axial anisotropy is almost the same, the transverse terms are significantly different. Indeed, the axial zero-field splitting parameter D of Fe8Br turned out to be only 2.5% higher than that of Fe8pcl. This difference further reduces if the fourth-order $B_4{}^0$ term is considered. On the other hand a 10% increase is observed in the rhombic term E of Fe8pcl. This made Fe8pcl an ideal candidate to investigate the role of the transverse anisotropy on the quantum tunneling of the magnetization. In detail, the larger transverse terms observed in Fe8pcl compared to original Fe8Br produce a lower effective energy barrier for the former, and result in a faster relaxation. This phenomenon was indeed observed in both the ac susceptibility measurements and dc relaxation measurements, which pointed to a tunneling rate about 35 times larger in Fe8pcl than in Fe8Br.

5. The Mn4 family

A third family of SMMs which has been intensively studied comprises Mn4 clusters, whose structure is sketched in Fig. 10 [96]. The core can be described as a cubane $[Mn_4O_3X]^{6+}$ (where $X = MeCO_2{}^-, Cl^-, Br^-, N_3{}^-, NCO–, OH^-, MeO^-$), with three manganese(III) and one manganese(IV). The X group bridges the three manganese(III) ions. The coupling between the $S = 2$ and 3/2 spins is antiferromagnetic and the ground state has $S = 9/2$ [97]. Some of the members of the family have crystallographically imposed trigonal symmetry. The interest for this type of clusters is not limited to their SMM behavior. Actually they were first synthesised to model the manganese cluster present in water oxidizing complex of Photosystem II [98]. Oriented samples of $[Mn_4O_3Cl(O_2CMe)_3(dbm)_3]$, where Hdbm is dibenzoylmethane, provided sharp signals at 327.9 GHz which were analysed affording the crystal field parameters $D/k = -0.76$ K

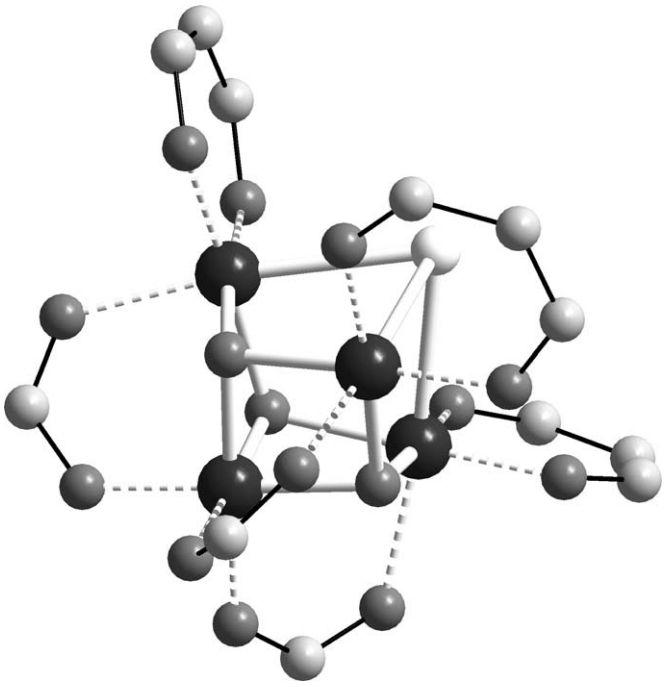

Fig. 10. Simplified view of the molecular structure of $[Mn_4O_3Cl(O_2CMe)_3(dbm)_3]$, evidencing the distorted cubane structure. Large black spheres: manganese atoms; small dark grey spheres: oxygen atoms; small light grey spheres: carbon atoms; white ball: chlorine atom.

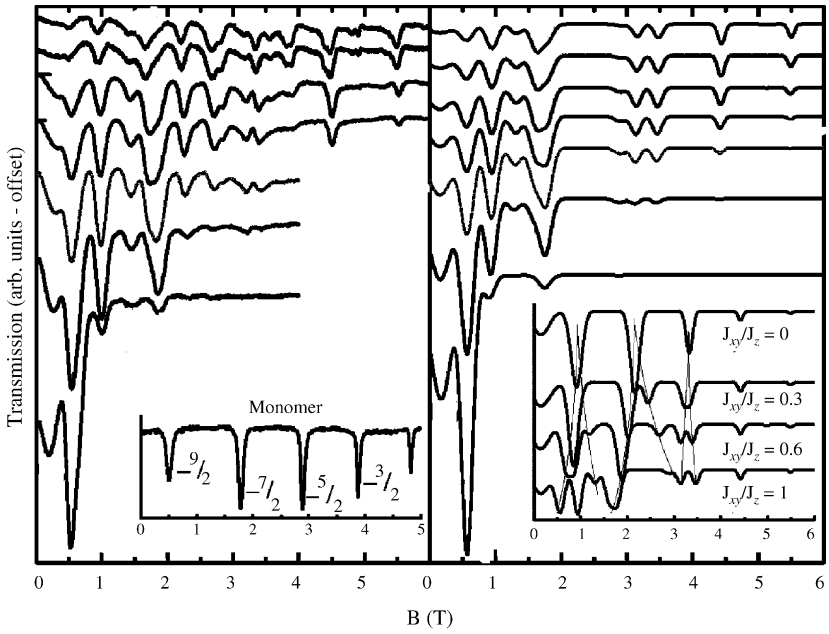

Fig. 11. (Left) Transmission EPR spectra (145 GHz) obtained for $[Mn_4O_3Cl_4(O_2CEt)_3(py)_3]_2$, $[Mn4]_2$ with static magnetic field applied along the easy axis at variable temperatures (from bottom to top: 2, 4, 6, 8, 10, 15 and 18 K). The inset shows a single 6 K, 140 GHz spectrum obtained for a monomeric Mn4 complex. (Right) Simulations of the dimer data obtained by using $D/k = -0.750$ K, $B_4{}^0/k = -5 \times 10^{-5}$ K, $g_z = 2$, and $J_{zz}/k = J_{xy}/k = J/k = 0.12$ K. The inset illustrates the effect of the transverse part of the exchange (J_{xy}) for four values of J_{xy}/J_z ($T = 8$ K). Adapted from ref. [102].

and $B_4^0/k = -1.1 \times 10^{-1}$ K [14] which were subsequently confirmed by INS data [99].

Some of the members of the Mn4 family show also the presence of sizeable intermolecular interactions. In particular, in the crystal structure of $[Mn_4O_3Cl_4(O_2CEt)_3(py)_3]_2$ Mn4 clusters are connected pairwise through C–H···Cl and Cl···Cl interactions [100]. The individual clusters have the typical $S = 9/2$ ground state. The interaction between them is taken into consideration by introducing a term:

$$H = J_z \widehat{S}_{1z} \cdot \widehat{S}_{2z} + J_{xy}(\widehat{S}_{1x} \cdot \widehat{S}_{2x} + \widehat{S}_{1y} \cdot \widehat{S}_{2y}) \quad (13)$$

where 1 and 2 refer to the two interacting clusters. The states of the dimer can be described by using $|M_1 M_2\rangle$ functions, 1 and 2 referring to the two clusters. The inclusion of the interaction term (13) determines a splitting of the resonances due to the fact that there are now two transitions allowed, namely from $|M_1 M_2\rangle$ to $|M_1 + 1, M_2\rangle$ and $|M_1, M_2 + 1\rangle$, respectively. The splittings have been measured at variable frequencies (in the range 136–144 GHz) [101], variable temperature spectra and simulations at 145 GHz are shown in Fig. 11 [102]. The analysis of the HF-EPR spectra further demonstrated that decoherence rates of the coupled states (i.e., in more conventional EPR terms, the electronic transverse relaxation rate T_2) are considerably smaller than the characteristic quantum splittings ($\Delta/h \sim$ GHz, where Δ is the energy splitting and h is the Planck constant) induced by the exchange couplings within the dimers. This was claimed by the authors to represent a step forward for potential applications involving molecular magnets.

6. Other SMMs

A class of SMMs based on iron(III) ions has the structure sketched in Fig. 12. The coupling between the central iron(III) and the three peripheral ions is antiferromagnetic in such a way that the ground state has $S = 5$. The first system reported to show SMM behaviour was $[Fe_4(OMe)_6(dpm)_6]$, where dpm is the anion of dipivaloylmethane [16]. The compound crystallizes in the monoclinic system, with a crystallographically imposed binary axis passing through the central iron(III) and one of the peripheral ions. The analysis of the magnetic data suggested a quasi axial ZFS with $D/k = -0.28$ K, and polycrystalline powder EPR spectra confirmed this view. Single crystal EPR spectra recorded at 95 GHz, however, revealed some complications [103]. In fact in a monoclinic cell where the molecule has C_2 symmetry only one signal per crystal orientation should be observed. However the signals showed clear splittings and indicated the presence of at least three inequivalent molecules. In fact the analysis of the X-ray data showed the presence of disorder due to the different wrapping of the bidentate ligands around the four iron(III) ions. The three different geometric isomers which are believed to exist in the crystal have the structure depicted in Fig. 13. Experimentally the AA, AB and BB isomers correspond to 49%, 42% and 9% of the molecules. Single crystal EPR spectra were then fitted with three different ZFS parameters: $D_{AA}/k = -0.296(1)$ K; $D_{AB}/k = -0.273(2)$ K and $D_{BB}/k = -0.252(2)$ K. The slight differences in D values are attributed to the small variation in the coordination environment provided by the oxygen donors which surround the metal ion.

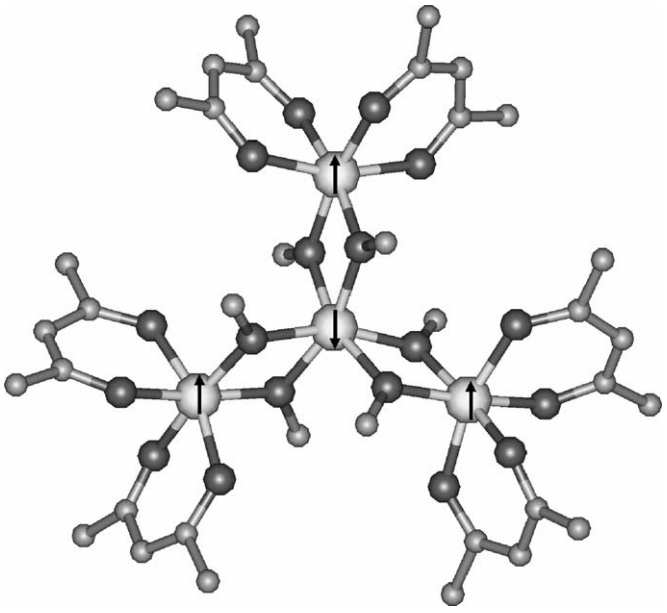

Fig. 12. Structure of $Fe_4(OMe)_6(dpm)_6$ cluster (Fe4). Large light grey balls: iron atoms; small medium grey balls: carbon atoms; small dark grey balls: oxygen atoms. Hydrogen atoms have been omitted for clarity sake. The arrows depicts the spin structure of the $S = 5$ ground state arising from the antiferromagnetic coupling of the $S = 5/2$ central iron with the external ones.

To overcome the problem of ligand disorder recently a new derivative of this cluster has been prepared, by substituting the six bridging methoxide ligands with two tripodal $thme^{3-}$ ligands

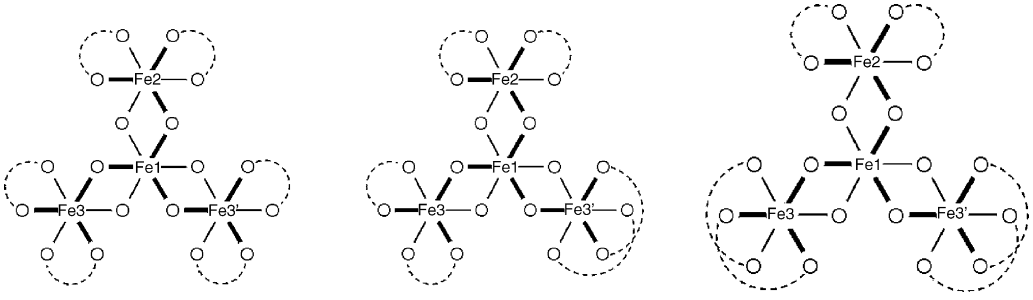

Fig. 13. Scheme of the three isomers of $Fe_4(OMe)_6(dpm)_6$ arising as a consequence of the two possible binding modes of the dpm anions on two peripheral iron centers. Adapted from ref. [103].

(H_3thme is tris(hydroxymethyl)ethane) [104]. The new cluster has a crystallographically imposed trigonal symmetry and – most remarkably – an enhanced anisotropy. HF-EPR spectra showed that the $|D|$ parameter is more than twice as large as in the parent cluster ($D/k = -0.64$ K versus -0.28 K). Consequently, SMM behaviour can be observed at higher temperatures ($\sim$2 K versus <1 K).

Different explanations have been proposed for this huge increase in anisotropy but all of them attribute a crucial role to the central iron [104,105]. This center undergoes two different types of distortion along the trigonal axis in both derivatives: namely a trigonal axial distortion and a trigonal rotation. These two effects are counterbalancing each other in the parent compound while they sum up in the thme derivative. As a consequence the contribution of this center to molecular anisotropy is enhanced in the thme derivative. However, the different anisotropy observed in the two variants cannot be ascribed solely to the central iron(III) ion. Indeed, if the experimental D value is related to the spin hamiltonian parameters of the four iron ions using Eq. (7) then the ZFS of the central iron should undergo a variation of ca. $-1.5\,cm^{-1}$ passing from Fe4dpm to Fe4thme, which is far too high. More subtle effects should then be active and these are currently under study through the synthesis and characterization of a family of closely related clusters [106]. This result illustrates how chemical changes can strongly influence the overall magnetic anisotropy via a modulation of the single ion properties. On this respect the importance of detailed studies on families of isostructural complexes cannot be overemphasized.

A new family of SMMs has been reported recently. It comprises four nickel(II) ions, $S_i = 1$, and has general formula $[Ni(hmp)(ROH)X]_4$, where R = Me, Et, etc., X = Cl, Br and hmp^- is the anion of 2-hydroxymethylpyridine. The nickel(II) ions are ferromagnetically coupled to give a ground $S = 4$ state [107]. SMM behaviour was observed with evidence of a bias field provided by the interactions between neighbouring clusters, akin to that observed in the Mn4 clusters described above. The clusters exhibit extremely fast magnetization quantum tunnelling (MQT) which in practice makes the direct measurement of relaxation by DC methods impossible.

The EPR spectra of the Ni4 clusters confirmed a negative ZFS parameter $D/k \sim -0.9$ K. A detailed analysis of the *t*-BuEtOH derivative using single crystal HF-EPR was possible due to the presence of very sharp lines. A doubling of the lines has been observed in the low temperature spectra of this cluster, which had been initially attributed to the exchange interaction between the clusters [108]. Subsequent studies pointed out that this phenomenon is associated with a structural phase transition observed at 46 K, leading to some disorder in *t*-BuEtOH ligand. Single crystal spectra measured in the hard plane showed that a sizeable fourth order transverse field is operative, giving rise to a large tunnel splitting and thus to fast tunnelling rate in zero magnetic field [109]. An accurate single crystal variable frequency study over $[Ni0.07Zn3.93(hmp)(ROH)X]_4$ derivative yielded the magnitude and orientations of the single ion zero field splitting tensors, demonstrating that a large tilting of single ion local axes with respect to the unique axis occurs and a large single ion transverse anisotropy is present [110].

7. Antiferromagnetic clusters

In the previous sections the attention was focussed on systems with a large spin in the ground state. Although SMMs represent an important class of molecular nanomagnets, it must be stressed that also antiferromagnetic clusters with a total spin of zero, or 1/2 in the ground state provide interesting aspects concerning quantum spins generated by coupling of many individual spins.

An example is provided by $K_6[V_{15}As_6O_{42}(H_2O)]\cdot 8H_2O$, V15, which contains fifteen oxovanadium(IV) ions, $S = 1/2$, arranged in three layers of 6, 3, and 6 magnetic ions, respectively [111]. The spin topology is schematically depicted in Fig. 14. The magnetic coupling is strongly antiferromagnetic in the layers of six ions, in such a way that at low temperature the spins in these hexagons are completely coupled. The three spins in the triangular layers on the other hand are only weakly coupled to give a ground manifold with two spin doublets and one spin quartet [112]. The magnetic properties at low temperature show hysteretic effects which depend on the detailed pattern of the energies of the low lying multiplets [113–116]. If the triangle is equilateral then the two spin doublets should be degenerate. However the degeneracy may be removed by phonon coupling, yielding geometrical distortions, or through spin orbit coupling (Dzyhaloshinsky–Moriya interactions). INS experiment seems to indicate that phonon coupling is dominant [117]. Frequency swept magnetic resonance spectroscopy experiments were performed using backward wave oscillators (BWO) which are coherent, monochromatic, frequency tunable

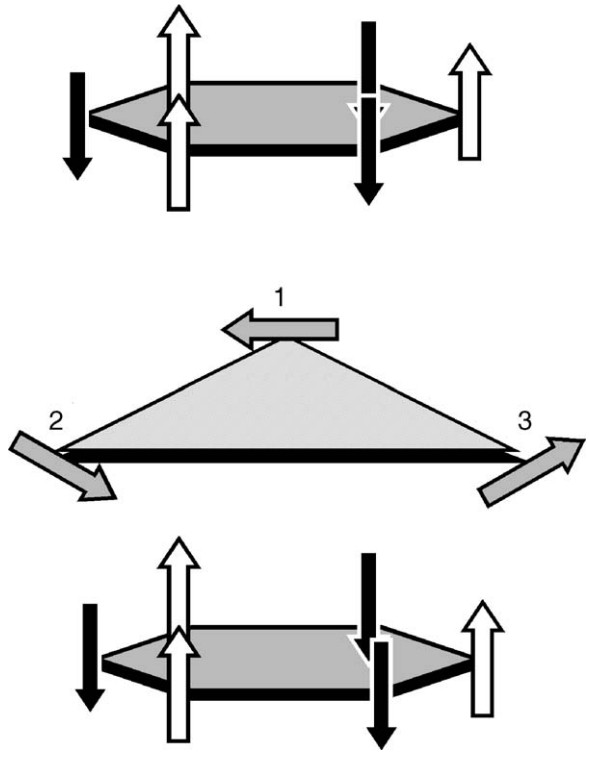

Fig. 14. Schematic spin structure of V15 cluster. A strong antiferromagnetic coupling is observed in the two hexagon layers, while weak coupling is observed in the triangular layer. Adapted from ref. [112].

radiation sources operating in the millimeter and submillimeter spectral range [118]. No signal was observed on varying the frequency in the range 1.5–10 cm^{-1} without an applied magnetic field. Applying an external magnetic field showed one transition shifting to higher frequencies on increasing the magnetic field. The spectra were assigned to transitions within the doublet levels and provided anisotropic g values, $g_{\|c} = 1.981(3)$ and $g_{\perp c} = 1.953(3)$, where c is the trigonal crystal axis [119]. In agreement with INS results the role of Dzyhaloshinsky–Moriya interactions seems to be negligible, thus making transitions between the ground doublets and the first excited quartet unobservable.

8. Antiferromagnetic rings

An important subgroup of molecular nanomagnets is represented by antiferromagnetic rings, which have been suggested to be useful materials for developing quantum computing techniques [120,121]. Also in this family there is an archetypal compound, namely a decanuclear iron(III) derivative of formula $[Fe(OMe)_2(O_2CCH_2Cl)]_{10}$, Fe10, which is commonly named the ferric wheel [122]. The ten iron(III) ions are antiferromagnetically coupled in such a way that the ground state is $S = 0$. The original interest for the ferric wheel was due to the observation of a stepped magnetisation at 0.7 K [123]. The origin of the steps is easily understood considering that excited stated with $S > 0$ are not too far from the ground state. In fact the lowest $S = 1$ state lies 4.3 cm^{-1} above the ground state in zero field. In a magnetic field the $M = -1$ component of the triplet decreases its energy as $-1g\mu_B H$, and in a critical field $H_c = \Delta/(g\mu_B)$ it becomes the ground state (Δ is the zero field separation between the $S = 0$ and the first-excited $S = 1$ multiplet). Similar considerations hold for the excited states with $S = 2$, 3, etc. up to 25. In pulsed magnetic fields it has been possible to observe the steps corresponding to cross-overs up to $S = 9$. This technique allows one to measure the energies of the excited states in a sort of spectroscopy. It is interesting to notice that the energies of the excited states have been found to follow a Landé interval rule:

$$E(S) = \left(\frac{J_{\text{eff}}}{2}\right) S(S+1) \tag{14}$$

where J_{eff} is an effective constant which is related to the J constant describing the nearest neighbour coupling by:

$$J_{\text{eff}} = \frac{4J}{N} \tag{15}$$

where N is the number of spins in the ring. Eqs. (14) and (15) are expected to better approximate the spin manifold the larger is the individual spin S_i and the smaller is N.

The inclusion of ZFS terms affects the critical fields H_c and introduces a dependence of H_c upon the orientation of the magnetic field with respect to the anisotropy axes. These effects have been carefully investigated for a smaller ring with rigorous axial symmetry, namely $[NaFe_6(OCH_3)_{12}(pmdbm)_6]ClO_4$ (hereafter Fe6), by means of cantilever torque magnetometry (CTM) [124] and inelastic neutron scattering [125]. It was then possible to obtain the axial ZFS parameter of the first excited $S = 1$ state ($D_1/k \sim 6.57$ K). HF-EPR was then applied to elucidate the origin of magnetic anisotropy in Fe6. In an elegant study, an isostructural Ga6 complex doped with a small fraction of Fe was used to obtain isolated paramagnetic ions in a diamagnetic host and thus directly measure the single ion ZFS parameters ($D/k = 0.62$ K, $E/k = 0.095$ K for Fe(III) by HF-EPR (110–525 GHz) [125]. It is interesting to note here that both the D parameter pertaining to the single ion and the global ones are positive. On the basis of the cantilever torque magnetometry results this was related to the combined action of the projection coefficient (which are negative) and of the orientation of the single ion anisotropy tensors, whose principal axes turned out to lie almost in the ring plane.

To the best of our knowledge, the only direct HF-EPR study on ferric wheel has been reported by Pilawa et al., who investigated the hexameric ferric wheel of $Fe_6(tea)_6$ [126,127]. High frequency (115–350 GHz), W-band and X-Band EPR single crystal spectra as a function of temperature (5–60 K) combined with the unusual sharpness of the observed lines (30–60 G) allowed them to assign signals to the excited spin states with $S = 1$–4. Spin Hamiltonian parameters were obtained through simulation for these four states ($D_1/k = 11.8$ K, $D_2/k = 1.23$ K, $D_3/k = 1.08$ K, $D_4/k \sim 0.63$ K). Exploiting the high symmetry (S_6) of the cluster it was possible to relate these values to the elementary parameters characterising the intramolecular interactions. In particular by calculating the dipolar interaction (0.075 K) it was possible to obtain an evaluation of the isotropic exchange constant ($J/k = 31.5$ K) and of the projection of the single ion zero field splitting for Fe^{III} ions ($D_{zz}/k = -0.40$ K) along the cluster symmetry axis. On the other hand, the high symmetry made it impossible to obtain more detailed information concerning the principal values and directions of the single ion zero field splitting term.

Another antiferromagnetic ring which has been accurately investigated is $[Cr_8F_8Piv_{16}]$, Cr8, where Piv is pivaloate. The compound, which has the structure shown in Fig. 15, crystallizes in two different space groups, depending on the solvent used for crystallisation. One of the two phases is tetragonal, Cr8t [128], and the other monoclinic, Cr8m [129]. The magnetic susceptibility goes through a maximum at around 40 K for both compounds, and the temperature dependence of χ was fitted with a unique coupling constant $J = 12.1$ cm^{-1} for Cr8t and $J = 11.9$ cm^{-1} for Cr8m. These values were found to be consistent with those reported for similar compounds. The antiferromagnetic coupling between chromium(III) ions ($S_i = 3/2$) suggests an $S = 0$ ground state with the first excited $S = 1$ state at 6.70 cm^{-1} and the first $S = 2$ state at 20.1 cm^{-1}. The energy of the $S = 1$ state was confirmed by cantilever torque magnetometry, CTM, which showed a transition from $S = 0$ to 1 at a field of ca. 7 T. From the fitting of the experimental data the singlet triplet separation was estimated to be 6.51 cm^{-1}, with a zero field splitting of the triplet parameterised by $D = 1.59$ cm^{-1}. Polycrystalline powder EPR spectra were reported at 115 and 230 GHz, in the range 1.6–25 K. The signal corresponding to the $S = 1$ and 2 lowest lying states were observed, yielding $D_1 = 1.63$ cm^{-1} and $D_2 = 0.37$ cm^{-1}, respectively. D_1 is in excellent agreement with the value obtained from CTM data [128].

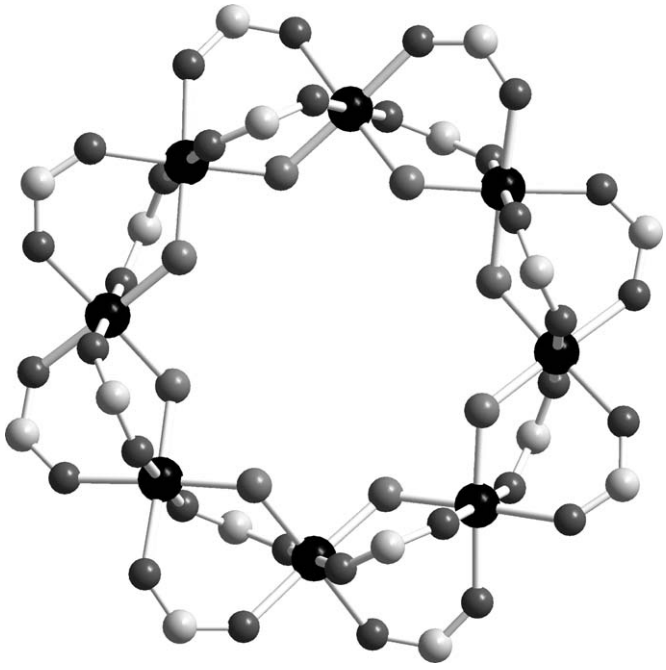

Fig. 15. Molecular structure of $Cr_8F_8Piv_{16}$, Cr8. Large black spheres: chromium atoms; small dark grey spheres: oxygen atoms; small medium grey spheres: fluorine atoms; small light grey spheres: carbon atoms. Hydrogen atoms have been omitted for clarity sake.

Additional evidence on the nature of the low lying states was obtained through inelastic neutron scattering and heat capacity measurements. The value of the coupling constant obtained through INS is 11.8 cm^{-1}. Detailed calculations including low symmetry components provided the eigenvectors thus showing that in the ground $S=0$ state there is some admixing with $S=2$, $M=0$, while the $S=1$ state is admixed with the $S=3$ state [130,131].

Even membered antiferromagnetic rings are relatively common nowadays, while odd membered rings are still extremely rare [132], with the exception of the systems with three members. This is unfortunate because the odd membered rings are expected to give rise to interesting phenomena due to spin frustration effects. In fact it is expected that in odd membered rings the low lying states are largely degenerate in such a way that the magnetic properties at low temperature are very rich.

Recently Winpenny et al. developed a suitable strategy for forming odd membered rings starting from even membered rings. The key idea is very simple as sketched in Fig. 16. The

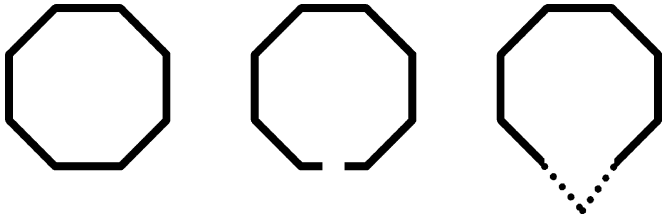

Fig. 16. Schematic of the process leading to the formation of an odd membered ring. Starting from an octanuclear wheel (left), the even membered ring is broken (center) and an additional metallic center is inserted (right).

even membered ring is broken and an additional ion is inserted. Success was achieved by starting from Cr8, yielding a ring containing eight Cr^{III} ions ($S=3/2$) and one Ni^{II} ion ($S=1$), Cr8Ni (Fig. 15), of formula $[(C_6H_{11})_2NH_2][Cr_8NiF_9(Piv)_{18}]$ [133,134]. The Cr8Ni contains an even number of unpaired electrons thus allowing a diamagnetic ground state, which is indeed observed by magnetic measurements, and can not be considered a typical example of a frustrated system; at the same time, however, its spin topology is such that not all the antiferromagnetic interactions can be simultaneously satisfied and therefore some frustration is present. On this respect the system can be regarded as a magnetic analogue of the Mobius strip: the odd number of spins makes it impossible for all spins to align anti-parallel to their nearest neighbour—as preferred where the exchange is anti ferromagnetic. The region where the spins cannot be arranged anti-parallel to each other can be considered as the "knot" of the Mobius strip whereas the flat region of the strip occurs where the neighbouring spins are alternately "up and down", thus satisfying the antiferromagnetic interactions. Whether the "knot" is localized on nickel(II) centre or on the chromium(III) chain strictly depends on the ratio between J_{CrCr} and J'_{CrNi} and HF-EPR played a crucial role in the resolution of this problem. Indeed, if $J' < J$ the first excited state $S=1$ is mainly composed by nickel(II) contribution and one expects $g_{S=1} \cong 2.2$. On the other hand if $J' > J$ the knot is delocalized over the chromium(III) chain and the $S=1$ excited state is well described by an antiferromagnetic coupling between a $S_{Cr}=2$ spin resulting from coupling of the eight Cr spins and the $S=1$ of the Ni. By using appropriate spin projection techniques [42] it is possible to find quantitative relations between the g values of the ring and those of the individual ions. This would result in $g_{S=1} = c_1 g_{Cr} - c_2 g_{Ni}$. Assuming $g_{Cr}=1.97$ and $g_{Ni}=2.2$ yields $g_{S=1}=1.86$. HF-EPR spectra recorded at different frequencies and temperatures showed indeed that the lowest lying paramagnetic state is characterized by $g=1.86$, thus unequivocally indicating that $J' > J$ and the knot is delocalized over the chromium(III) chain.

9. Double exchange

In all the compounds discussed so far the interaction between the magnetic centres is dominated by the so-called superexchange interaction, which is an adequate description in the case of essentially localized electrons. Matters become different in mixed valence compounds in which the barrier to electron transfer is small. In this case a strong stabilisation is observed for the state which does not require spin flip. This effect is called double exchange [135–137]. Perhaps this point becomes clearer using as an example a dinuclear nickel compound originally reported by Sacconi et al. in the 1970s [138]. $[Ni_2(napy)_4X_2]^+$, where napy is the chelating ligand 1,8-naphthyridine, and X = Cl, Br, I [139]. The total charge of the Ni_2 unit is 3+, suggesting a mixed valence Ni^{I}–Ni^{II}. X-ray data did not show any significant difference between the coordination environments of the two metal ions, suggesting a Class III or Class II mixed valence compound in the classification of Robin and Day [140]. Early magnetic data showed that the ground state has $S=3/2$ with no evidence of excited states with smaller S. The double exchange justification

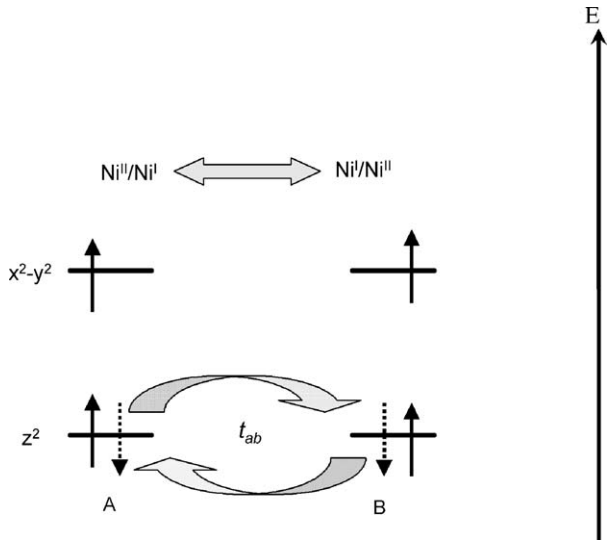

Fig. 17. Energy level scheme for d^8 and d^9 nickel ions in square pyramidal coordination environments and mechanism of the double exchange. The magnetic orbitals are indicated as dz^2 and $dx^2 - y^2$. If one electron of the originally d^9 ion hops from the dz^2 orbital to the analogous one of the d^8 site it must keep its spin antiparallel to that of the other electron in the dz^2 orbital, thus stabilizing a quartet spin state like an effective ferromagnetic coupling between localized d^8 and d^9 ions.

is depicted in Fig. 17. Ni^{II} has $S = 1$ and Ni^{I} has $S = 1/2$. The transfer of one electron from the z^2 orbital of Ni^{I} to that of Ni^{II} occurs keeping the spin parallel to that of the electrons in the x^2–y^2 orbitals, thus justifying the ground $S = 3/2$ state.

In a spin Hamiltonian approach the energies of the states can be described by:

$$E\pm = \left(\frac{J}{2}\right) S(S+1) \pm B\left(\frac{S+1}{2}\right) \quad (16)$$

where '±' refers to the two states which originate from the mixed valence nature of the compound, $S = 1/2, 3/2$, B is the parameter describing the double exchange:

$$B = \frac{t_{ab}}{2S_0 + 1} \quad (17)$$

t_{ab} is the transfer integral of the z^2 orbitals and S_0 is the spin of the centre without the extra electron. DFT calculations have recently confirmed this qualitative scheme giving $B = 3261\ cm^{-1}$ and $J = 952\ cm^{-1}$ for the iodide derivative. The isotropic coupling is antiferromagnetic and it is only the ferromagnetic double exchange contribution which stabilizes the ground $S = 3/2$ state [141].

Early EPR spectra at X-band showed that the splitting of the $S = 3/2$ state is large compared to the microwave quantum of $0.3\ cm^{-1}$. In fact only the transitions within the $M = \pm 1/2$ Kramers doublet is observed, with $g_{\parallel} = 2.18$, $g_{\perp} = 4.13$. These are the g values of an effective Hamiltonian with $S_{eff} = 1/2$, for which $g_{\parallel eff} = g_{\parallel}$, $g_{\perp eff} = 2g_{\perp}$. No transitions involving the $M = \pm 3/2$ Kramers doublet were observed [142]. Polycrystalline powder EPR spectra recorded at 245 GHz, shown in Fig. 18, showed a wealth of transitions which were fitted with $g_{\parallel} = 2.18$, $g_{\perp} = 2.12$, $D = -2.7\ cm^{-1}$. A detailed analysis was attempted, but no safe conclusion could be reached on the origin of this large ZFS [141]. It is tempting to consider that the mixed valence nature of the system has something to do with it. On this respect it would be a very interesting strategy that of designing a mixed valence SMM with small barrier to electron transfer, so as to induce double exchange effect.

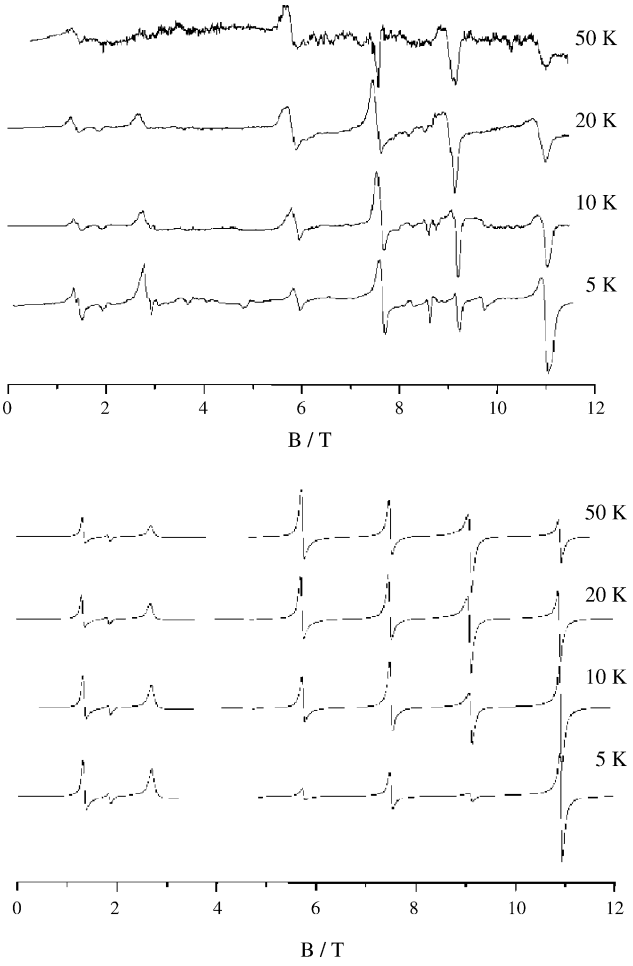

Fig. 18. Experimental (upper) HF-EPR (245 GHz) spectra of $[Ni_2(napy)_4I_2]^+$ as a function of temperature and best simulation spectra with parameters reported in the text (lower). Adapted from ref. [141].

10. Conclusions

EPR spectroscopy is a very powerful tool for the investigation of the low lying levels of molecular nanomagnets. The recent developments in high frequency high field experiments have really opened many exciting perspectives to look in detail at the nature of the low lying spin levels which have such a fundamental role in determining the properties of molecular nanomagnets.

Twin techniques can be considered—the zero field EPR (which is a particular case of frequency swept magnetic resonance spectroscopy, FSMRS) and inelastic neutron scattering. Both of them have the advantage of being zero field techniques thus giving a more direct access to the energy pattern of the spin multiplets. On the other hand the possibility given by HF-EPR

of varying both the frequency and the field allows an easy separation between field dependent and field independent terms of the spin Hamiltonian. INS has also the advantage of exploring transitions obeying the selection rules $\Delta S = 0, \pm 1$, $\Delta M = \pm 1$, thus providing the opportunity to observe transitions involving different total spin multiplets. However, one major disadvantage of this technique is that large amounts of deuterated samples are often needed.

Standard EPR, where the oscillating magnetic field of the radiation is perpendicular to the static field, explores $\Delta M = \pm 1$ transitions. It is possible to perform experiments also using a parallel configuration of the static and oscillating magnetic field exploring the $\Delta M = 0$ transitions. The technique has long been used in the investigation of so called EPR silent ions, like iron(II), which have importance in biological systems [143,144], or Mn(III) [145]. Recently parallel mode X-band EPR spectroscopy has been used to investigate the low lying levels of a dodecanuclear chromium(III) cluster which has a ground $S = 6$ state [146].

Electron magnetic resonance is not the only resonance technique which is conveniently used in the investigation of molecular nanomagnets. Another technique which has provided good direct insight into the properties of molecular nanomagnets is nuclear magnetic resonance (NMR). The experiments are generally performed in solid, either polycrystalline powders or single crystals and have given information on the relaxation of the magnetisation, on the spin density distribution at the magnetic nuclei, on the tunnel effects and on the mixing of low lying spin levels [147–164]. Similar information has also been obtained using muons in muon spin resonance (μSR) [165–168].

Acknowledgments

The financial support of MIUR (FIRB and PRIN projects) and of EC through several programs (QueMolNa, MolNanoMag and SENTINEL) is gratefully acknowledged.

References

[1] The National Nanotechnology Initiative Strategic Plan [Web Page] Available at. http://www.nano.gov/NNI_Strategic_Plan_2004.pdf.
[2] A.J. Leggett, in: L. Gunther, B. Barbara (Eds.), Quantum tunneling of magnetization-QTM'94, Kluwer, Dordrecht, 1995, p. 1.
[3] P.C.E. Stamp, Nature 383 (1996) 125.
[4] S.H. Sun, C.B. Murray, J. Appl. Phys. 85 (1999) 4325.
[5] C.T. Black, C.B. Murray, R.L. Sandstrom, S.H. Sun, Science 290 (2000) 1131.
[6] F.X. Redl, K.S. Cho, C.B. Murray, S. O'brien, Nature 423 (2003) 968.
[7] T. Lis, Acta Cryst. B36 (1980) 2042.
[8] A. Caneschi, D. Gatteschi, R. Sessoli, A.-L. Barra, L.C. Brunel, M. Guillot, J. Am. Chem. Soc. 113 (1991) 5873.
[9] R. Sessoli, D. Gatteschi, A. Caneschi, M.A. Novak, Nature (Lond.) 365 (1993) 141.
[10] R. Sessoli, H.L. Tsai, A.R. Schake, S.Y. Wang, J.B. Vincent, K. Folting, D. Gatteschi, G. Christou, D.N. Hendrickson, J. Am. Chem. Soc. 115 (1993) 1804.
[11] G. Aromi, S.M.J. Aubin, M.A. Bolcar, G. Christou, H.J. Eppley, K. Folting, D.N. Hendrickson, J.C. Huffman, R.C. Squire, H.L. Tsai, S. Wang, M.W. Wemple, Polyhedron 17 (1998) 3005.
[12] D. Gatteschi, R. Sessoli, J. Villain, Molecular Nanomagnets, Oxford University Press, Oxford, 2006.
[13] A.L. Barra, P. Debrunner, D. Gatteschi, Ch.E. Schulz, R. Sessoli, Europhys. Lett. 35 (1996) 133.
[14] S.M.J. Aubin, N.R. Dilley, L. Pardi, J. Krzystek, M.W. Wemple, L.C. Brunel, M.B. Maple, G. Christou, D.N. Hendrickson, J. Am. Chem. Soc. 120 (1998) 4991.
[15] S.L. Castro, Z.M. Sun, C.M. Grant, J.C. Bollinger, D.N. Hendrickson, G. Christou, J. Am. Chem. Soc. 120 (1998) 2365.
[16] A.L. Barra, A. Caneschi, A. Cornia, F.F. De Biani, D. Gatteschi, C. Sangregorio, R. Sessoli, L. Sorace, J. Am. Chem. Soc. 121 (1999) 5302.
[17] A.L. Barra, A. Caneschi, D. Gatteschi, D.P. Goldberg, R. Sessoli, J. Solid State Chem. 145 (1999) 484.
[18] J. Yoo, E.K. Brechin, A. Yamaguchi, M. Nakano, J.C. Huffman, A.L. Maniero, L.C. Brunel, K. Awaga, H. Ishimoto, G. Christou, D.N. Hendrickson, Inorg. Chem. 39 (2000) 3615.
[19] J.C. Goodwin, R. Sessoli, D. Gatteschi, W. Wernsdorfer, A.K. Powell, S.L. Heath, A.L. Barra, J. Chem. Soc. Dalton Trans. (2000) 4702.
[20] C. Boskovic, E.K. Brechin, W.E. Streib, K. Folting, D.N. Hendrickson, G. Christou, Chem. Commun. (2001) 467.
[21] L.F. Jones, E.K. Brechin, D. Collison, M. Helliwell, T. Mallah, S. Piligkos, G. Rajaraman, W. Wernsdorfer, Inorg. Chem. 42 (2003) 6601.
[22] E.C. Yang, N. Harden, W. Wernsdorfer, L. Zakharov, E.K. Brechin, A.L. Rheingold, G. Christou, D.N. Hendrickson, Polyhedron 22 (2003) 1857.
[23] S. Osa, T. Kido, N. Matsumoto, N. Re, A. Pochaba, J. Mrozinski, J. Am. Chem. Soc. 126 (2004) 420.
[24] M. Soler, W. Wernsdorfer, K. Folting, M. Pink, G. Christou, J. Am. Chem. Soc. 126 (2004) 2156.
[25] M. Murugesu, M. Habrych, W. Wernsdorfer, K.A. Abboud, G. Christou, J. Am. Chem. Soc. 126 (2004) 4766.
[26] M. Murrie, S.J. Teat, H. Stoeckli-Evans, H.U. Gudel, Angew. Chem. Int. Ed. 42 (2003) 4653.
[27] N. Aliaga-Alcalde, R.S. Edwards, S.O. Hill, W. Wernsdorfer, K. Folting, G. Christou, J. Am. Chem. Soc. 126 (2004) 12503.
[28] E.C. Sanudo, W. Wernsdorfer, K.A. Abboud, G. Christou, Inorg. Chem. 43 (2004) 4137.
[29] G. Chaboussant, R. Basler, H.U. Gudel, S. Ochsenbein, A. Parkin, S. Parsons, G. Rajaraman, A. Sieber, A.A. Smith, G.A. Timco, R.E.P. Winpenny, Dalton Trans. (2004) 2758.
[30] C.M. Zaleski, E.C. Depperman, J.W. Kampf, M.L. Kirk, V.L. Pecoraro, Angew. Chem. Int. Ed. 43 (2004) 3912.
[31] H. Oshio, N. Hoshino, T. Ito, M. Nakano, J. Am. Chem. Soc. 126 (2004) 8805.
[32] A. Caneschi, D. Gatteschi, N. Lalioti, C. Sangregorio, R. Sessoli, G. Venturi, A. Vindigni, A. Rettori, M.G. Pini, M.A. Novak, Angew. Chem. Int. Ed. 40 (2001) 1760.
[33] T. Kajiwara, M. Nakano, Y. Kaneko, S. Takaishi, T. Ito, M. Yamashita, A. Igashira-Kamiyama, H. Nojiri, Y. Ono, N. Kojima, J. Am. Chem. Soc. 127 (2005) 10150.
[34] M. Ferbinteanu, H. Miyasaka, W. Wernsdorfer, K. Nakata, K. Sugiura, M. Yamashita, C. Coulon, R. Clerac, J. Am. Chem. Soc. 127 (2005) 3090.
[35] E. Pardo, R. Ruiz-Garcia, F. Lloret, J. Faus, M. Julve, Y. Journaux, F. Delgado, C. Ruiz-Perez, Adv. Mater. 16 (2004) 1597.
[36] N.E. Chakov, W. Wernsdorfer, K.A. Abboud, G. Christou, Inorg. Chem. 43 (2004) 5919.
[37] H. Miyasaka, R. Clerac, K. Mizushima, K. Sugiura, M. Yamashita, W. Wernsdorfer, C. Coulon, Inorg. Chem. 42 (2003) 8203.
[38] R. Clerac, H. Miyasaka, M. Yamashita, C. Coulon, J. Am. Chem. Soc. 124 (2002) 12837.
[39] L. Bogani, C. Sangregorio, R. Sessoli, D. Gatteschi, Angew. Chem. Int. Ed. 44 (2005) 5817.
[40] J.S. Miller, M. Drillon (Eds.), Magnetism: Molecules to Materials: Models and Experiments, vol. 1, Wiley-VCH, Weinheim, 2001.
[41] A. Cornia, D. Gatteschi, R. Sessoli, Coord. Chem. Rev. 219 (2001) 573.

[42] A. Bencini, D. Gatteschi, EPR of Exchange Coupled Systems, Springer-Verlag, Berlin, 1990.
[43] A.L. Barra, L.C. Brunel, D. Gatteschi, L. Pardi, R. Sessoli, Acc. Chem. Res. 31 (1998) 460.
[44] M.J. Mombourquette, J.A. Weil, J. Magn. Reson. 99 (1992) 37.
[45] S. Stoll, A. Schweiger, J. Magn. Reson. 178 (2006) 42.
[46] C.J.H. Jacobsen, E. Pedersen, J. Villadsen, H. Weihe, Inorg. Chem. 32 (1993) 1216.
[47] G.R. Hanson, K.E. Gates, C.J. Noble, M. Griffin, A. Mitchell, S. Benson, J. Inorg. Biochem. 98 (2004) 903.
[48] W.R. Hagen, Coord. Chem. Rev. 192 (1999) 209.
[49] V.A. Igonin, O.I. Shchegolikhina, S.V. Lindeman, M.M. Levitsky, Y.T. Struchkov, A.A. Zhdanov, J. Organomet. Chem. 423 (1992) 351.
[50] A. Cornia, A.C. Fabretti, D. Gatteschi, G. Palyi, E. Rentschler, O.I. Shchegolikhina, A.A. Zhdanov, Inorg. Chem. 34 (1995) 5383.
[51] E. Rentschler, D. Gatteschi, A. Cornia, A.C. Fabretti, A.-L. Barra, O.I. Shchegolikhina, A.A. Zhdanov, Inorg. Chem. 35 (1996) 4427.
[52] G.L. Abbati, A. Caneschi, A. Cornia, A.C. Fabretti, Y.A. Pozdniakova, O.I. Shchegolikhina, Angew. Chem. Int. Ed. 41 (2002) 4517.
[53] H. Blok, S.B. Disselhorst Jajm, J. Orlinskii, Schmidt, J. Magn. Reson. 166 (2004) 92.
[54] G.M. Smith, J.C.G. Lesurf, R.H. Mitchell, P.C. Riedi, Rev. Sci. Instrum. 70 (1998) 1787.
[55] M. Mola, S. Hill, P. Goy, M. Gross, Rev. Sci. Instrum. 71 (2000) 186.
[56] B. Cage, S.E. Russek, D. Zipse, N.S. Dalal, J. Appl. Phys. 97 (2005) 10M507.
[57] K. Petukhov, W. Wernsdorfer, A.L. Barra, V. Mosser, Phys. Rev. B 72 (2005).
[58] A.L. Barra, D. Gatteschi, R. Sessoli, Phys. Rev. B 56 (1997) 8192.
[59] A. Abragam, B. Bleaney, Electron Paramagnetic Resonance of Transition Ions, Dover, New York, 1986.
[60] J. Van Slageren, S. Vongtragool, B. Gorshunov, A.A. Mukhin, N. Karl, J. Krzystek, J. Telser, A. Müller, C. Sangregorio, D. Gatteschi, M. Dressel, Phys. Chem. Chem. Phys. 5 (2003) 3837.
[61] A.A. Mukhin, V.D. Travkin, A.K. Zvezdin, S.P. Lebedev, A. Caneschi, D. Gatteschi, Europhys. Lett. 44 (1998) 778.
[62] M. Hennion, L. Pardi, I. Mirebeau, E. Suard, R. Sessoli, A. Caneschi, Phys. Rev. B: Condens. Matter 56 (1997) 8819.
[63] I. Mirebeau, M. Hennion, H. Casalta, H. Andres, H.U. Güdel, A.V. Irodova, A. Caneschi, Phys. Rev. Lett. 83 (1999) 628.
[64] S. Hill, J.A.A.J. Perenboom, N.S. Dalal, T. Hathaway, T. Stalcup, J.S. Brooks, Phys. Rev. Lett. 80 (1998) 2453.
[65] S. Hill, R.S. Edwards, S.I. Jones, N.S. Dalal, J.M. North, Phys. Rev. Lett. 90 (2003) 217204.
[66] A.H. Morrish, The Physical Principles of Magnetism, John Wiley & Sons, Inc., New York, 1966.
[67] L. Thomas, F. Lionti, R. Ballou, D. Gatteschi, R. Sessoli, B. Barbara, Nature (Lond.) 383 (1996) 145.
[68] J.R. Friedman, M.P. Sarachik, J. Tejada, R. Ziolo, Phys. Rev. Lett. 76 (1996) 3830.
[69] E.M. Chudnovsky, D.A. Garanin, Phys. Rev. Lett. 8718 (2001) 7203.
[70] A. Cornia, R. Sessoli, L. Sorace, D. Gatteschi, A.L. Barra, C. Daiguebonne, Phys. Rev. Lett. 89 (2002) 257201.
[71] A. Cornia, A.C. Fabretti, R. Sessoli, L. Sorace, D. Gatteschi, A.L. Barra, C. Daiguebonne, T. Roisnel, Acta Crystallogr. Sect. C: Cryst. Struct. Commun. 58 (2002) m371.
[72] S. Takahashi, R.S. Edwards, J.M. North, S. Hill, N.S. Dalal, Phys. Rev. B 70 (2004) 094429.
[73] R. Amigo, E. del Barco, Ll. Casas, E. Molins, J. Tejada, I.B. Rutel, B. Mommouton, N. Dalal, J. Brooks, Phys. Rev. B 65 (2002) 172403.
[74] E. Del Barco, A.D. Kent, S. Hill, J.M. North, N.S. Dalal, E.M. Rumberger, D.N. Hendrickson, N. Chakov, G. Christou, J. Low Temp. Phys. 140 (2005) 119.
[75] S. Hill, R.S. Edwards, J.M. North, S. Maccagnano, N.S. Dalal, Polyhedron 22 (2003) 1897.
[76] K. Petukhov, S. Hill, N.E. Chakov, K.A. Abboud, G. Christou, Phys. Rev. B 70 (2004) 054426.
[77] G. Chaboussant, A. Sieber, S. Ochsenbein, H.U. Gudel, M. Murrie, A. Honecker, N. Fukushima, B. Normand, Phys. Rev. B 70 (2004) 104422.
[78] K. Takeda, K. Awaga, T. Inabe, A. Yamaguchi, H. Ishimoto, T. Tomita, H. Mitamura, T. Goto, N. Mori, H. Nojiri, Phys. Rev. B 65 (2002) 094424.
[79] P.D. Boyd, Q. Li, V.B. Vincent, K. Folting, H.-R. Chang, W.E. Streib, J.C. Huffman, G. Christou, D.N. Hendrickson, J. Am. Chem. Soc. 110 (1988) 8537.
[80] Y.-G. Wei, S.-W. Zhang, M.-C. Shao, Y.-Q. Tang, Polyhedron 16 (1997) 1471.
[81] D. Ruiz, Z. Sun, B. Albela, K. Folting, J. Ribas, G. Christou, D.N. Hendrickson, Angew. Chem. Int. Ed. Engl. 37 (1998) 300.
[82] Z.M. Sun, D. Ruiz, E. Rumberger, C.D. Incarvito, K. Folting, A.L. Rheingold, G. Christou, D.N. Hendrickson, Inorg. Chem. 37 (1998) 4758.
[83] K. Takeda, K. Awaga, T. Inabe, Phys. Rev. B 57 (1998) R11062.
[84] J. An, Z.-D. Chen, J. Bian, J.-T. Chen, S.-X. Wang, S. Gao, G.-X. Xu, Inorg. Chim. Acta 299 (2000) 28.
[85] S.M.J. Aubin, Z.M. Sun, H.J. Eppley, E.M. Rumberger, I.A. Guzei, K. Folting, P.K. Gantzel, A.L. Rheingold, G. Christou, D.N. Hendrickson, Inorg. Chem. 40 (2001) 2127.
[86] M. Pacchioni, A. Cornia, A.C. Fabretti, L. Zobbi, D. Bonacchi, A. Caneschi, G. Chastanet, D. Gatteschi, R. Sessoli, Chem. Comm. (2004) 2604.
[87] H.-L. Tsai, H.J. Eppley, N. de Vries, K. Folting, G. Christou, D.N. Hendrickson, J. Chem. Soc. Chem. Commun. (1994) 1745.
[88] H.J. Eppley, H.L. Tsai, N. Devries, K. Folting, G. Christou, D.N. Hendrickson, J. Am. Chem. Soc. 117 (1995) 301.
[89] S.M.J. Aubin, Z. Sun, L. Pardi, J. Krzystek, K. Folting, L.-C. Brunel, A.L. Rheingold, G. Christou, D.N. Hendrickson, Inorg. Chem. 38 (1999) 5329.
[90] K. Wieghardt, K. Pohl, I. Jibril, G. Huttner, Angew. Chem. Int. Ed. Engl. 23 (1984) 77.
[91] C. Sangregorio, T. Ohm, C. Paulsen, R. Sessoli, D. Gatteschi, Phys. Rev. Lett. 78 (1997) 4645.
[92] A.L. Barra, D. Gatteschi, R. Sessoli, Chem. Eur. J. 6 (2000) 1608.
[93] S. Hill, S. Maccagnano, K. Park, R.M. Achey, J.M. North, N.S. Dalal, Phys. Rev. B 65 (2002) 224410.
[94] D. Zipse, J.M. North, N.S. Dalal, S. Hill, R.S. Edwards, Phys. Rev. B 68 (2003).
[95] A.L. Barra, F. Bencini, A. Caneschi, D. Gatteschi, C. Paulsen, C. Sangregorio, R. Sessoli, L. Sorace, Chemphyschem 2 (2001) 523.
[96] S.Y. Wang, K. Folting, W.E. Streib, E.A. Schmitt, J.K. Mccusker, D.N. Hendrickson, G. Christou, Angew. Chem. Int. Ed. 30 (1991) 305.
[97] S. Wang, H.-L. Tsai, E. Libby, K. Folting, W.E. Streib, D.N. Hendrickson, G. Christou, Inorg. Chem. 35 (1996) 7578.
[98] J.S. Bashkin, H.-R. Chang, W.E. Streib, J.C. Huffman, D.N. Hendrickson, G. Christou, J. Am. Chem. Soc. 109 (1987) 6502.
[99] H. Andres, R. Basler, H.U. Gudel, G. Aromi, G. Christou, H. Buttner, B. Ruffle, J. Am. Chem. Soc. 122 (2000) 12469.
[100] W. Wernsdorfer, N. Allaga-Alcalde, D.N. Hendrickson, G. Christou, Nature 416 (2002) 406.
[101] R.S. Edwards, S. Hill, S. Bhaduri, N. Aliaga-Alcalde, E. Bolin, S. Maccagnano, G. Christou, D.N. Hendrickson, Polyhedron 22 (2003) 1911.
[102] S. Hill, R.S. Edwards, N. Aliaga-Alcalde, G. Christou, Science 302 (2003) 1015.
[103] A. Bouwen, A. Caneschi, D. Gatteschi, E. Goovaerts, D. Schoemaker, L. Sorace, M. Stefan, J. Phys. Chem. B 105 (2001) 2658.
[104] A. Cornia, A.C. Fabretti, P. Garrisi, C. Mortalo, D. Bonacchi, D. Gatteschi, R. Sessoli, L. Sorace, W. Wernsdorfer, A.L. Barra, Angew. Chem. Int. Ed. 43 (2004) 1136.
[105] J. Ribas-Arino, T. Baruah, M.R. Pederson, J. Chem. Phys. 123 (2005) 044303.
[106] Accorsi, A.-L. Barra, A. Caneschi, G. Chastanet, A. Cornia, A.C. Fabretti, D. Gatteschi, C. Mortalò, R. Sessoli, L. Sorace, W. Wernsdorfer, L. Zobbi, J. Am. Chem. Soc. 128 (2006) 4742–4755.

[107] E.C. Yang, W. Wernsdorfer, S. Hill, R.S. Edwards, M. Nakano, S. Maccagnano, L.N. Zakharov, A.L. Rheingold, G. Christou, D.N. Hendrickson, Polyhedron 22 (2003) 1727.
[108] R.S. Edwards, S. Maccagnano, E.C. Yang, S. Hill, W. Wernsdorfer, D. Hendrickson, G. Christou, J. Appl. Phys. 93 (2003) 7807.
[109] C. Kirman, J. Lawrence, S. Hill, E.C. Yang, D.N. Hendrickson, J. Appl. Phys. 97 (2005).
[110] E.C. Yang, C. Kirman, J. Lawrence, L.N. Zakharov, A.L. Rheingoid, S. Hill, D.N. Hendrickson, Inorg. Chem. 44 (2005) 3827.
[111] A. Müller, J. Döring, Angew. Chem. Int. Ed. Engl. 27 (1988) 1721.
[112] D. Gatteschi, L. Pardi, A.-L. Barra, A. Müller, J. Döring, Nature 354 (1991) 463.
[113] I. Chiorescu, W. Wernsdorfer, B. Barbara, A. Müller, H. Bögge, J. Appl. Phys. 87 (2000) 5496.
[114] I. Chiorescu, W. Wernsdorfer, A. Müller, H. Bögge, B. Barbara, Phys. Rev. Lett. 84 (2000) 3454.
[115] I. Chiorescu, W. Wernsdorfer, A. Müller, H. Bögge, B. Barbara, J. Magn. Magn. Mater. 221 (2000) 103.
[116] I. Chiorescu, W. Wernsdorfer, A. Müller, S. Miyashita, B. Barbara, Phys. Rev. B 67 (2003) 020402.
[117] G. Chaboussant, S.T. Ochsenbein, A. Sieber, H.U. Gudel, H. Mutka, A. Müller, B. Barbara, Europhys. Lett. 66 (2004) 423.
[118] A.A. Volkov, Yu.G. Goncharov, G.V. Kozlov, A.A. Mukhin, A.M. Prokhorow, Infrared Phys. 25 (1985) 369.
[119] S. Vongtragool, B. Gorshunov, A.A. Mukhin, J. Van Slageren, M. Dressel, A. Müller, Phys. Chem. Chem. Phys. 5 (2003) 2778.
[120] F. Meier, J. Levy, D. Loss, Phys. Rev. B 68 (2003) 134417.
[121] F. Troiani, M. Affronte, S. Carretta, P. Santini, G. Amoretti, Phys. Rev. Lett. 94 (2005).
[122] K.L. Taft, S.J. Lippard, J. Am. Chem. Soc. 112 (1990) 9629.
[123] K.L. Taft, C.D. Delfs, G.C. Papaefthymiou, S. Foner, D. Gatteschi, S.J. Lippard, J. Am. Chem. Soc. 116 (1994) 823.
[124] A. Cornia, A.G.M. Jansen, M. Affronte, Phys. Rev. B 60 (1999) 12177.
[125] G.L. Abbati, L.C. Brunel, H. Casalta, A. Cornia, A.C. Fabretti, D. Gatteschi, A.K. Hassan, A.G.M. Jansen, A.L. Maniero, L.A. Pardi, C. Paulsen, U. Segre, Chem. Eur. J. 7 (2001) 1796.
[126] B. Pilawa, R. Desquiotz, M.T. Kelemen, M. Weickenmeier, A. Geisselmann, J. Magn. Magn. Mater. 177–181 (1997) 748.
[127] B. Pilawa, I. Keilhauer, R. Bofinger, D. Marinov, S. Knorr, A. Grupp, Appl. Magn. Reson. 21 (2001) 527.
[128] J. Van Slageren, R. Sessoli, D. Gatteschi, A.A. Smith, M. Helliwell, R.E.P. Winpenny, A. Cornia, A.L. Barra, A.G.M. Jansen, E. Rentschler, G.A. Timco, Chem. Eur. J. 8 (2002) 277.
[129] N.V. Gerbeleu, I.T. Struchkov, G.A. Timko, A.S. Batsanov, K.M. Indrichan, G.A. Popovich, Doklady Akademii Nauk Sssr 313 (1990) 1459.
[130] M. Affronte, T. Guidi, R. Caciuffo, S. Carretta, G. Amoretti, J. Hinderer, I. Sheikin, A.G.M. Jansen, A.A. Smith, R.E.P. Winpenny, J. Van Slageren, D. Gatteschi, Phys. Rev. B 68 (2003) 104403.
[131] S. Carretta, J. Van Slageren, T. Guidi, E. Liviotti, C. Mondelli, D. Rovai, A. Cornia, A.L. Dearden, F. Carsughi, M. Affronte, C.D. Frost, R.E.P. Winpenny, D. Gatteschi, G. Amoretti, R. Caciuffo, Phys. Rev. B 67 (2003) 094405.
[132] C.S. Campos-Fernandez, R. Clerac, J.M. Koomen, D.H. Russell, K.R. Dunbar, J. Am. Chem. Soc. 123 (2001) 773.
[133] O. Cador, D. Gatteschi, R. Sessoli, F.K. Larsen, J. Overgaard, A.L. Barra, S.J. Teat, G.A. Timco, R.E.P. Winpenny, Angew. Chem. Int. Ed. 43 (2004) 5196.
[134] O. Cador, D. Gatteschi, R. Sessoli, A.L. Barra, G.A. Timco, R.E.P. Winpenny, J. Magn. Magn. Mater. 290 (2005) 55.
[135] C. Zener, Phys. Rev. 82 (1951) 403.
[136] P.W. Anderson, H. Hasegawa, Phys. Rev. 100 (1955) 675.
[137] J.-J. Girerd, J. Chem. Phys. 79 (1983) 1766.
[138] D. Gatteschi, C. Mealli, L. Sacconi, J. Am. Chem. Soc. 95 (1973) 2736.
[139] L. Sacconi, C. Mealli, D. Gatteschi, Inorg. Chem. 13 (1974) 1985.
[140] M.B. Robin, P. Day, Adv. Inorg. Chem. Radiochem. 10 (1967) 247.
[141] A. Bencini, E. Berti, A. Caneschi, D. Gatteschi, E. Giannasi, I. Invernizzi, Chem. Eur. J. 8 (2002) 3660.
[142] A. Bencini, D. Gatteschi, L. Sacconi, Inorg. Chem. 17 (1978) 2670.
[143] N. Gupta, F. Bonomi, D.M. Kurtz, N. Ravi, D.L. Wang, B.H. Huynh, Biochemistry 34 (1995) 3310.
[144] M.F.J.M. Verhagen, W.G.B. Voorhorst, J.A. Kolkman, R.B.G. Wolbert, W.R. Hagen, FEBS Lett. 336 (1993) 13.
[145] K.A. Campbell, D.A. Force, P.J. Nixon, F. Dole, B.A. Diner, R.D. Britt, J. Am. Chem. Soc. 122 (2000) 3754.
[146] S. Piligkos, D. Collison, V.S. Oganesyan, G. Rajaraman, G.A. Timco, A.J. Thomson, R.E.P. Winpenny, E.J.L. Mc Innes, Phys. Rev. B 69 (2004) 134424.
[147] D. Gatteschi, A. Lascialfari, F. Borsa, J. Magn. Magn. Mater. 185 (1998) 238.
[148] A.G. Harter, N.E. Chakov, R. Achey, A. Reyes, P. Kuhns, G. Christou, N.S. Dalal, Polyhedron 24 (2005) 2346.
[149] A.G. Harter, N.E. Chakov, B. Roberts, R. Achey, A. Reyes, P. Kuhns, G. Christou, N.S. Dalal, Inorg. Chem. 44 (2005) 2122.
[150] A. Lascialfari, Z.H. Jang, F. Borsa, D. Gatteschi, A. Cornia, J. Appl. Phys. 83 (1998) 6946.
[151] M.H. Julien, Z.H. Jang, A. Lascialfari, F. Borsa, M. Horvatic, A. Caneschi, D. Gatteschi, Phys. Rev. Lett. 83 (1999) 227.
[152] T. Goto, T. Koshiba, T. Kubo, K. Awaga, Phys. Rev. B 67 (2003) 104408.
[153] Z.H. Jang, A. Lascialfari, F. Borsa, D. Gatteschi, Phys. Rev. Lett. 84 (2000) 2977.
[154] Y. Furukawa, K. Watanabe, K. Kumagai, Z.H. Jang, A. Lascialfari, F. Borsa, D. Gatteschi, Phys. Rev. B 62 (2000) 14246.
[155] Y. Furukawa, K. Kumagai, A. Lascialfari, S. Aldrovandi, F. Borsa, R. Sessoli, D. Gatteschi, Phys. Rev. B 6409 (2001) 4439.
[156] R.M. Achey, P.L. Kuhns, A.P. Reyes, W.G. Moulton, N.S. Dalal, Phys. Rev. B 64 (2001) 4420.
[157] Y. Furukawa, K. Watanabe, K. Kumagai, F. Borsa, D. Gatteschi, Phys. Rev. B 64 (2001) 4401.
[158] J.K. Jung, D. Procissi, Z.H. Jang, B.J. Suh, F. Borsa, M. Luban, P. Kogerler, A. Müller, J. Appl. Phys. 91 (2002) 7391.
[159] Y. Furukawa, K. Watanabe, K. Kumagai, F. Borsa, T. Sasaki, N. Kobayashi, D. Gatteschi, Phys. Rev. B 67 (2003) 064426.
[160] Y. Furukawa, K. Watanabe, K. Kumagai, F. Borsa, D. Gatteschi, Phys. B Condens. Matter 329 (2003) 1146.
[161] Y. Furukawa, K. Aizawa, K. Kumagai, R. Ullu, A. Lascialfari, F. Borsa, J. Appl. Phys. 93 (2003) 7813.
[162] T. Kubo, T. Goto, T. Koshiba, K. Takeda, K. Awaga, Phys. Rev. B 65 (2002) 224425.
[163] Y. Furukawa, S. Kawakami, K. Kumagai, S.H. Baek, F. Borsa, Phys. Rev. B 68 (2003) 180405.
[164] P. Santini, S. Carretta, G. Amoretti, T. Guidi, R. Caciuffo, A. Caneschi, D. Rovai, Y. Qiu, J.R.D. Copley, Phys. Rev. B 71 (2005) 184405.
[165] A. Lascialfari, D. Gatteschi, F. Borsa, A. Shastri, Z.H. Jang, P. Carretta, Phys. Rev. B 57 (1998) 514.
[166] S.J. Blundell, F.L. Pratt, I.M. Marshall, C.A. Steer, W. Hayes, J.F. Letard, S.L. Heath, A. Caneschi, D. Gatteschi, Synth. Met. 133 (2003) 531.
[167] S.J. Blundell, in: J.S. Miller, M. Drillon (Eds.), Magnetism: Molecules to Materials, Wiley-VCH, Weinheim, 2001, p. 235.
[168] A. Lascialfari, R. Ullu, M. Affronte, F. Cinti, A. Caneschi, D. Gatteschi, D. Rovai, M.G. Pini, A. Rettori, J. Magn. Magn. Mater. 272-76 (2004) 1052.